5-2017

Trihalomethane, Dihaloacetonitrile, and Total N-nitrosamine Precursor Adsorption by Carbon Nanotubes: The Importance of Surface Oxides and Pore Volume

Erin Needham
University of Arkansas, Fayetteville

Trihalomethane, Dihaloacetonitrile, and Total *N*-nitrosamine Precursor Adsorption by Carbon Nanotubes: The Importance of Surface Oxides and Pore Volume

A thesis submitted in partial fulfillment
of the requirements for the degree of
Master of Science in Civil Engineering

by

Erin Michelle Needham
University of Arkansas
Bachelor of Science in Civil Engineering, 2013

May 2017
University of Arkansas

This thesis is approved for recommendation to the Graduate Council.

_____
Dr. Julian Fairey
Thesis Director

_____
Dr. Wen Zhang
Committee Member

_____
Dr. Justin Chimka
Committee Member

Abstract

As drinking water sources become increasingly impaired, enhanced removal of natural organic matter (NOM) may be required to curb formation of disinfection byproducts (DBPs) upon chlor(am)ination. While carbon nanotubes (CNTs) can adsorb NOM, their properties for DBP precursor adsorption have not been elucidated. Nine types of CNTs were assessed for trihalomethane (THM), dihaloacetonitrile (DHAN), and total *N*-nitrosamine (TONO) precursor adsorption. Batch isotherm experiments were completed with lake water and, to simulate an impaired condition, effluent from a wastewater treatment plant (WWTP). Adsorption varied with CNT type and dose, with TONO precursors having the highest percent removals from WWTP effluent (up to 97%). Physicochemical properties of CNTs were characterized by gas adsorption isotherms and x-ray photoelectron spectroscopy and numerical models were developed to identify CNT properties driving DBP precursor adsorption. The models fits were strong ($R^2 >$ 0.92) and indicated removal of the three precursor types increased with percent carboxyl groups ($p < 0.01$) and, for TONO precursors only, cumulative pore volume (CPV, $p = 0.001$). A multicollinearity analysis suggested surface oxides – particularly carboxyl groups – on the CNTs increased CPV, presumably by increasing electrostatic repulsive forces, which enhanced microporosity sufficiently to overshadow any repulsion of DBP precursors from negatively charged surface oxides. A size exclusion analysis revealed all CNT pores were accessible to TONO precursors, while THM and DHAN precursors had limited access to the smaller micropores. These findings provide a framework to modify CNTs to optimize adsorption of DBP precursors and demonstrate the potential of CNTs for TONO precursor removal.

Acknowledgements

I would like to thank my husband along with my family and friends for their encouragement and unwavering support. I would also like to acknowledge my thesis director and committee members for their guidance. Financial support from the National Science Foundation (CBET #1254350 to Julian Fairey) and the University of Arkansas Graduate School Doctoral Academy Fellowship is gratefully acknowledged.

Table of Contents

List of Published Papers

Needham, E. M., Sidney, S. M., Chimka, J. R., and Fairey, J. L., 2016. Trihalomethane, dihaloacetonitrile, and total *N*-nitrosamine precursor adsorption by carbon nanotubes: the importance of surface oxides and pore volume. Environmental Science: Water Research and Technology, 2 (6), 1004-1013.

1. Introduction

The tunable physicochemical properties of carbon nanotubes (CNTs) (Tawfick et al., 2012; De Volder et al., 2014) have the potential to be exploited in drinking water treatment plants (DWTPs) to adsorb organic precursors of disinfection byproducts (DBPs). While CNT toxicity (Liu et al., 2013; Das et al., 2014) is a concern in water treatment, the technology is now available to grow CNTs on various substrates as well as to incorporate CNTs into membrane filtration systems (De Volder et al., 2014). This may alleviate problems associated with fate and transport of toxic substances related to CNTs (Yang and Xing, 2009) in drinking waters. However, before CNT-based attached growth or membrane applications can be developed specifically to enhance DBP precursor removal, fundamental investigations are needed to quantify the affinity of CNTs for important groups of DBP precursors and elucidate the physiochemical properties primarily responsible for their adsorption.

It is well known that natural organic matter (NOM) in source water reacts with disinfectants (i.e., free chlorine or chloramines) to form DBPs at low $\mu g \cdot L^{-1}$ levels, such as trihalomethanes (THMs) (Rook, 1976) and dihaloacetonitriles (DHANs) (Krasner et al., 2006). In waters enriched with algal organic matter or impacted by wastewater treatment plant (WWTP) effluents, *N*-nitrosamines can also form, albeit at low $ng \cdot L^{-1}$ levels (Krasner et al., 2013). *N*-nitrosamines are a non-halogenated group of DBPs under consideration for regulation in drinking waters due to their high toxicity (Hrudey and Charrois, 2012). While the majority of *N*-nitrosamine research to date has focused on *N*-nitrosodimethylamine (NDMA) due to its prevalence in drinking water systems (Russell et al., 2012), recent studies have demonstrated NDMA may only comprise ~5% of total *N*-nitrosamines (TONO) in chloramine systems (Dai and Mitch, 2013). As such, relatively little is known about the removal of TONO precursors by

engineered sorbents, although a recent study demonstrated that they have some affinity for activated carbon (Dai et al., 2012). Further, the authors are aware of no studies that have assessed the concomitant removal of THM, DHAN, and TONO precursors in sorption processes. With respect to CNTs, other researchers have demonstrated their affinity for various NOM fractions in water (Wang et al., 2009; Yang and Xing, 2009), although these investigations were geared towards minimizing NOM uptake by CNTs to maximize adsorption of other target compounds. Regardless, development of novel sorbents with enhanced affinities for organic DBP precursors could potentially be leveraged to curb DBP formation in finished drinking waters, regardless of the disinfection scheme used.

As DBP measurements are time- and labor-intensive, reliable DBP precursor surrogate measures can be valuable screening tools to assess treatment. Previous studies by this research group have demonstrated metrics from fluorescence excitation-emission matrices (EEMs) collected before and after treatment but prior to chlor(am)ination were strong total THM (TTHM) precursor surrogates (Pifer and Fairey, 2014). In these studies, the EEMs were decomposed by parallel factor analysis (PARAFAC) to identify principal fluorophore groups (Stedmon and Bro, 2008). The corresponding maximum intensity values, F_{MAX}, of humic- and fulvic-like fluorophores correlated strongly with TTHM precursor concentrations. A more recent study found strong correlations between fluorescence intensity values from peak-picking (i.e., excitation-emission pairs, $I_{Ex/Em}$) and removal of TTHM and DHAN precursors (Do et al., 2015). There is, however, a strong basis for why fluorescence may be useful as a TONO precursor surrogate. For example, in contrast to EPA Method 521 *N*-nitrosamines, algal-derived organic matter is a strong precursor to uncharacterized *N*-nitrosamines measured by the TONO assay (Krasner et al., 2013). Additionally, Liao and colleagues found strong correlations between the

removal of NA9FP – the sum of the FP of the six N-nitrosamines regulated under the UCMR2 along with *N*-nitrosomorpholine, *N*-nitrosopiperidine, and *N*-nitrosodiphenylamine – and the regions of a fluorescence EEM associated with aromatic proteins (R = 0.88) and soluble microbial products (R = 0.90) (Liao et al., 2014). Aromatic proteins are nitrogen-containing and *N*-nitrosamine precursors can be present as functional groups, while soluble microbial products have been identified as an NDMA precursor (Krasner et al., 2013). In essence, secondary, tertiary, and quaternary amines may not fluoresce themselves but may be associated with compounds that do so. Coupled with the labor-intensive nature of TONOFP tests, a fluorescence-based TONO precursor surrogate would advance development of control measures for these DBPs.

Given that the structure of CNTs is equivalent to that of a rolled graphene sheet, their physicochemical properties dictate their functionality. CNTs can be produced in single-walled (SW) and multi-walled (MW) varieties, both of which have high specific surface area and range in hydrophobicity (Wang et al., 2009; Yang and Xing, 2009), size (Balasubramanian and Burghard, 2005), shape (De Volder et al., 2014), texture (Birch et al., 2013), defects (Shih and Li, 2008), and functionalities (Cho et al., 2008), all of which can be manipulated for their intended application. The ability to fine-tune CNT properties is an attractive option for use as a sorbent in drinking water treatment, but it is not yet known what properties are desirable for DBP precursor removal. Adsorption by CNTs is based on accessible surface area, which includes aggregated pores and large external surface area, in contrast to activated carbon, which preferentially adsorbs lower molecular weight compounds due to size exclusion from micropores. CNTs have been shown to have high adsorption capacities for organic contaminants

(Ren et al., 2011) and to outperform other microporous adsorbents in competitive adsorption systems (Upadhyayula et al., 2009).

The objective of this study is to assess physicochemical CNT properties for enhanced TTHM-, DHAN-, and TONO-precursor adsorption. Nine commercially available CNTs were selected with a variety of characteristics and used in batch isotherm tests with two diverse water sources – a well-characterized lake water (Sen et al., 2007) that serves as a drinking water source and an effluent from a conventional WWTP. The TTHM-, DHAN-, and TONO-precursor concentrations in the raw and CNT-treated waters were indirectly measured using a recently verified DBP formation potential (DBPFP) test (Do et al., 2015), modified from Standard Methods 5710-B and D (Eaton, 2005). Each CNT type was characterized physically by gas adsorption isotherms to determine their specific surface area and pore volume distributions, and chemically by x-ray photoelectron spectroscopy (XPS) to determine the relative composition of surface functional groups. These physicochemical properties were used as primary variables in models to assess the adsorption of TTHM-, DHAN-, and TONO-precursors. Modeling results revealed strong correlations between CNT properties and removal of all three DBP precursor types. The findings of this study provide guidance for selective modification of CNTs for enhanced DBP precursor adsorption.

2. Materials and Methods

2.1. Site Description and Sample Collection

Waters used for the isotherm experiments originated from Beaver Lake, the drinking water source for Northwest Arkansas, and the West Side Wastewater Treatment Plant (WS-EFF) in Fayetteville, AR. Beaver Lake water (BL-RAW) was collected at the intake structure of the Beaver Water District DWTP (Lowell, AR) on July 7, 2014. Details on the land use and nutrient

inputs in the Beaver Lake watershed can be found elsewhere (Sen et al., 2007). WS-EFF samples were collected June 6, 2014 from the WWTP effluent. The plant utilizes biological nutrient removal, depth filtration, and ultraviolet disinfection with effluent aeration prior to discharge. Raw water characteristics are detailed in Table S1. Both waters were stored in 50-L low-density polyethylene carboys at 4 °C in the dark prior to use in the isotherm experiments.

2.2. Experimental Procedures

2.2.1. Bottle-Point Isotherms

Bottle-point isotherms were conducted with nine types of commercially available CNTs, selected to cover a range of wall type (SW and MW), diameter, and length (Table S2). CNTs were added to the sample waters at doses of 0-, 25- and 50 $mg \cdot L^{-1}$, in triplicate, in 1.25 L headspace-free amber glass bottles and were tumbled end-over-end for 3 days. Lu et al. (2007) showed that 4 hours was sufficient to reach equilibrium in a bottle-point isotherm study with MWCNTs and NOM-spiked waters. An equilibrium time of 3 days (i.e., 18 times longer) was chosen in this study and assumed to be a sufficient equilibration period for all precursors given the diversity of DBP precursors in the sample waters, including those for TONO for which little characterization information exists. The pH drift during the 3 days of tumbling was less than 0.1 pH unit from the initial values reported in Table S1. CNT doses were chosen to achieve less than 100% removal based on preliminary TTHMFP and DHANFP removal tests, the results of which are detailed in Table S3. It is important to note that the goal of this study does not include determination of the required CNT doses at a DWTP; rather, this study is intended identify CNT properties for enhanced DBP precursor adsorption and future studies will focus on development of an optimized CNT type and application mode. Following tumbling, BL-RAW samples were filtered through pre-rinsed 0.45-μm polyethersulfone (PES) membranes (Karanfil et al., 2003).

The WS-EFF samples were passed through pre-rinsed 0.7-µm glass fiber filters prior to 0.45-µm PES filtration, as direct filtration with the PES membranes was impractically slow. In both cases, filtration removed all CNTs from the water samples, which was confirmed by the lower chlorine residuals (or higher demand) of the blank relative to the CNT-treated waters (Table S4). Methods used for measuring dissolved organic carbon (DOC) and fluorescence EEMs, and performing PARAFAC analysis are in the Supplementary Information (SI) in Appendix 1.

2.2.2. DBPFP

The procedure developed by Do et al. (2015) was used to assess the DBPFP of untreated waters (i.e., samples not exposed to CNTs) and CNT-treated waters and is detailed in the SI. EPA Method 551.1 with modifications (Pifer and Fairey, 2012) was used to extract TTHMs and DHANs into *n*-pentane. A gas chromatograph equipped with an electron capture detector (GC-ECD, Shimadzu 2010) was used to quantify TTHMFP (the sum of trichloromethane, dichlorobromomethane, dibromochloromethane, and tribromomethane formation potential) and DHANFP (the sum of dichloroacetonitrile, bromochloroacetonitrile, and dibromoacetonitrile formation potential). Details regarding the GC standard curve are provided in the SI. Blanks and check standards complied with EPA Method 551.1.

Assessment of total *N*-nitrosamine formation potential (TONOFP) began with a modified SPE procedure from EPA Method 521, adapted from Kulshrestha et al. (2010) SPE columns were conditioned with methanol and Milli-Q water, and then 500 mL sample aliquots were pulled through the columns at a flow rate of 5 $mL \cdot min^{-1}$. Following 10 minutes of column aspiration, *N*-nitrosamines were eluted from the SPE columns using 12 mL of methanol. All remaining water was removed from the column extracts using a sodium sulfate drying column rinsed with an additional 3 mL of methanol; leached sodium sulfate was subsequently removed

with a 0.2 μm nominal pore size polytetrafluoroethylene syringe filter. Samples were concentrated to 1 mL in a 37 °C water bath using an evaporator with ultra high purity nitrogen gas and stored at -20 °C. To eliminate potential interferences, *S*-nitrosothiols and nitrite, if present, were quenched immediately before TONO measurement from sample extracts with 20 $g \cdot L^{-1}$ mercuric chloride in Milli-Q water and 50 $g \cdot L^{-1}$ sulfanilamide in 1 N HCl, respectively. Notably, ion chromatography results (Table S1) indicated no nitrite in raw waters (method detection limit, MDL = 0.008 $mg \cdot L^{-1}$). An Eco Physics CLD 88sp chemiluminescence NO detector was used to quantify *N*-nitrosamines in purified samples, as detailed in Mitch and Dai. (2012) TONO concentrations were determined using a five-point NDMA standard curve, which was rerun after every four samples to account for sample mass recoveries. To prevent sample carryover, blank spike samples were run between each sample. As untreated BL-RAW samples had average TONO concentrations of 33 $ng \cdot L^{-1}$ as NDMA, just above the MDL of this procedure, TONO was not measured for these CNT-treated samples.

2.2.3. CNT Characterization

CNT physical characteristics were measured rather than relying on manufacturer specifications (Table S2). The pore volume distribution and Brunauer-Emmett-Teller (BET) surface area of the CNTs were measured using a Quantachrome Nova 2200e Surface Area and Pore Size Analyzer using N_2 and CO_2 gas adsorption at 77 K and 273 K, respectively. Adsorption isotherms (Figure S1) were collected at partial pressures of 0.005-0.99 using step sizes of 0.011-0.095. Pore volume distributions (Figure S2) were calculated from the isotherms using a hybrid density functional theory model that assumed slit pore geometry for micropores and slit or cylindrical pore geometry for mesopores (Zhu et al., 2011). The BET surface area (S_{BET}) was calculated using the N_2 adsorption isotherm in the linear relative pressure range from

0.05-0.30. However, it should be noted that S_{BET} is calculated without regard for the information given about micropores by the CO_2 adsorption isotherm. As such, S_{BET} is more suitable for comparing the amount of specific surface area individual CNT types have relative to each other, rather than their absolute specific surface area (Zhu et al., 2011).

XPS measurements were performed on pristine CNTs using a PHI 5000 VersaProbe spectrometer with an AlKα source, and a vacuum of 10^{-8} Torr was maintained during analysis. Methods for the XPS data analysis are detailed in the SI and carbon spectra deconvolutions are shown in Figure S3.

2.2.4. Data Modeling

To assess the impact of physicochemical CNT characteristics on DBP precursor adsorption, a multivariate analysis was performed for the three groups of DBPs. DBPFP was expressed as a ratio, as the median of each triplicate sample to the median of each untreated sample – either BL-RAW or WS-EFF, as appropriate. The median was utilized, rather than the mean, due to its relative insensitivity to outliers. The potential undue influence on the mean caused by outliers in the data is exacerbated by small sample sizes (e.g., n=3) for a given CNT type and dose. The following independent variables are associated with each group of DBPs: DOC ratio, UV_{254} ratio, CNT dose, carbon-carbon bonds, alcohol groups, carbonyl groups, carboxyl groups, S_{BET}, and cumulative pore volume (CPV). A binary variable (called Water Type) distinguishing between water types was also included in models of TTHM and DHAN Ratio. A binary variable was deemed more appropriate than including water quality characteristics as individual independent variables because these characteristics do not vary among the samples of a given water type. This variable was only used for TTHM and DHAN Ratio because TONO Ratio does not include samples of BL-RAW that were below the MDL.

DOC and UV_{254} ratio were calculated using procedures analogous to DBP ratio and were incorporated into the numerical models to assess their usefulness as DBP precursor surrogates, as opposed to the other independent variables related to CNT properties. An additional binary variable distinguishing single- and multi-walled CNTs is explored in the SI. Analysis of variance was used to study associations between DBP ratios and independent variables, or explanatory factors; equivalent linear regression was used to test hypotheses about factor levels while controlling for other factors. Models were estimated using STATA/IC 11.2 statistical software (StataCorp, 2009) which leverage principles of applied regression analysis as detailed by Draper and Smith (1998).

3. Results and Discussion

3.1. DBP Precursor Adsorption by CNTs

Figure 1 shows percent removals of TTHMFP and DHANFP from BL-RAW (Figure 1A) and of TTHMFP, DHANFP, and TONOFP from WS-EFF (Figure 1B) attributed to each of the nine CNT types. Removal of TONOFP is only provided for WS-EFF because the concentration was below the MDL in BL-RAW. DBPFP removal is assumed to be due to adsorption of DBP precursors by the CNTs. As expected, increasing the CNT dose from 25- to 50 $mg \cdot L^{-1}$ resulted in an increase in percent removal for each DBP precursor for all nine CNT types. For TTHM precursor removal, the CNT types assessed performed similarly or better on a percent basis than the activated carbons used by Najm and colleagues (1991) and Iriarte-Velasco et al. (2008). Additionally, Iriarte-Velasco and colleagues reported removal of DOC (a commonly used as a TTHM precursor surrogate) as 27.6 and 2.2 mg DOC g^{-1} GAC for two types of GAC tested. In comparison, the removal of DOC from BL-RAW ranged from 8.5-24.2 mg DOC g^{-1} CNT, while the removal from WS-EFF was 11.4-57.1 mg DOC g^{-1} CNT, depending on the CNT type.

DHAN can be formed through two pathways utilizing different reactants, which include: (1) the decarboxylation pathway, in which chloramine (and/or free chlorine) reacts with amine-containing moieties of NOM and (2) the aldehyde pathway, where an aldehyde incorporates chloramine-nitrogen (Shah and Mitch, 2012). For BL-RAW samples, the percent removals of DHAN precursors were less than that of TTHM precursors for all nine CNT types; in contrast, for WS-EFF samples, removal of DHAN precursors by CNT Types 1, 2, and 8 surpassed removal of TTHM precursors. Though other precursors in natural waters may contribute to DHANFP in an unknown degree, this relative difference in precursor removal between BL-RAW and WS-EFF suggests the possibility either the amine- or aldehyde-based precursors are more prevalent in WS-EFF and have a greater affinity for CNTs than the less abundant precursors.

Average percent removal of TONO precursors reached a maximum of 93% (Type 9) at a CNT dose of 25 $mg \cdot L^{-1}$ and 97% at the higher CNT dose. Because of a lack of similar studies involving CNTs and TONO precursors, direct comparisons to the literature are not possible. However, using linear interpolation, we compared these results to Hanigan et al. (2012) who quantified NDMA precursor adsorption in batch studies with activated carbon and found that 6 of the 9 CNT types achieved approximately the same or higher percent removals of TONO precursors on a mass sorbent basis. It is important to note that NDMA may only comprise ~5% of TONO formed following chloramination of wastewater effluent organic matter (Dai and Mitch, 2013) and little is known about the physicochemical properties of TONO precursors relative to NDMA precursors. Additionally, the average percent removal of TONO precursors at the 50 $mg \cdot L^{-1}$ CNT dose was 31% greater than either TTHM or DHAN precursor removal. Hydrophilic base fractions of organic matter are considered the most likely *N*-nitrosamine precursors in DWTPs (Wang et al., 2013) and WWTP effluent (Pehlivanoglu-Mantas and

Sedlak, 2008). Taken together, this may indicate that CNTs can sorb both hydrophobic and hydrophilic NOM fractions from natural waters although additional testing is required to support such an assertion. Regardless, the results in Figure 1B illustrate that many CNT types have high affinities for TONO precursors, the underlying reasons for which are discussed further in Section 3.3.

3.2. CNT Characterization

The physical and chemical characteristics of each CNT type are summarized in Table 1. The shape of the gas adsorption isotherms (Figure S1) indicated the nitrogen adsorption isotherms were IUPAC Type II and the carbon dioxide adsorption isotherms were Type I (Sing et al., 1985; Zhang et al., 2010; Adeniran and Mokaya, 2015). CPV varied almost one order of magnitude, from 0.135 $cm^3 \cdot g^{-1}$ (Type 7) to 1.267 $cm^3 \cdot g^{-1}$ (Type 2). The CPV measurements of all CNT types fell within the range of values reported in the literature (0.104-2.46 $cm^3 \cdot g^{-1}$), which vary based on CNT dimensions and the number of walls and are associated with both pristine and modified CNTs (Zhang et al., 2010; Adeniran and Mokaya, 2015; Apul and Karanfil, 2015). Pore volume distributions were bimodal (Figure S2), with microporosity assumed to be associated with the interstitial space within CNT bundles and mesoporosity associated with the space within individual tubes (Yang et al., 2005). S_{BET} measurements (Table 1) were within 55% of supplier specifications (Table S2) in all cases with the exception of Type 2, which was 106% greater. In fact, S_{BET} for Type 2 (837 $m^2 \cdot g^{-1}$) was higher than the range reported in the literature for SWCNTs (22-662 $m^2 \cdot g^{-1}$) (Zhang et al., 2010; Birch et al., 2013). However, S_{BET} can vary based on CNT dimensions and the methods of synthesis and purification, and thus, values outside the ranges reported in the literature are not unexpected. For all MWCNT types, S_{BET} fell within the range reported in the literature (58-653 $m^2 \cdot g^{-1}$) (Cho et al., 2008; Zhang et al., 2010;

Birch et al., 2013; Apul and Karanfil, 2015). Elemental composition data from deconvolution of carbon spectra from XPS measurements (Figure S3) indicated that surface oxides (i.e., the sum of C-O, C=O, and COO functional groups) comprised 11% (Type 7) to 14% (Type 2) of the CNTs (Table 1), which falls into the range (6-32%) reported by others (Ago et al., 1999; Komarova et al., 2015). In Section 3.3, we explore relationships between CNT properties and DBP precursor adsorption.

3.3. Impacts of Physicochemical CNT Properties on DBP Precursor Adsorption

Multivariate analysis for each DBP type yielded regression coefficients and p-values (Table 2) for TTHM (n = 36), DHAN (n = 36) and TONO (n = 18). Coefficients with $p < 0.05$ are assumed to be nonzero and indicate a significant effect on DBP ratio (i.e., influent-normalized effluent concentration), controlling for other variables in the model. Significance of an independent variable in the negative direction indicates that an increase in the magnitude of that variable resulted in a decrease in DBP ratio, otherwise stated as an increase in the removal of that DBP precursor by the nine CNT types. A scatterplot of residuals versus fitted values suggested constant error variance (Figures 2A, B, and C). R-squared values indicated strong correlations between fitted values and observed values of DBP ratio for TTHM ($R^2 = 0.92$, Figure 2D), DHAN ($R^2 = 0.92$, Figure 2E) and TONO ($R^2 = 0.96$, Figure 2F). In essence, the model has no discernible bias to the magnitude of DBP ratio and at least 92% of the variation is explained by the measured CNT properties.

The regression coefficients and p-values in Table 2 indicate several notable trends. Opposing signs of significance for the Water Type binary variable for TTHM Ratio and DHAN Ratio indicate that in comparing DBP precursor removal from the two waters, there was greater removal of (1) TTHM precursors from BL-RAW and (2) DHAN precursors from WS-EFF

samples when controlling for all other variables in the model. Also, across all three DBP groups, an increase in either CNT dose or the amount of carboxyl groups resulted in greater removal of precursors. That CNT dose shows this trend only confirms the effect of these particular dosages illustrated in Figure 1. However, the relationship between DBP ratio and the percent of carboxyl groups is intriguing due to the significance of that variable across all DBP groups and suggests that CNT surface chemistry is important for DBP precursor adsorption. For TONO Ratio only, a positive correlation with the percent of alcohol functional groups indicates a decrease in the amount of those surface oxides increased adsorption of TONO precursors. Additionally, for TONO Ratio alone, there was a significant relationship with CPV, indicating that an increase in CPV resulted in enhanced TONO precursor removal. Notably, true relationships between DBP precursor removal and CNT surface chemistry would be obscured by large errors in XPS carbon spectra deconvolution or any other independent variable. The risk of accidentally or randomly observing a relationship that is untrue is kept low by the choice of significance level (alpha = 0.05). Therefore, we have confidence in the importance of significant chemical characteristics in the models.

Surface oxides are generally considered to inhibit sorption of NOM (i.e., DBP precursors) to activated carbon due to repulsion caused by their negative surface charge (Karanfil et al., 2007). However, the results of the multivariate model (Table 2) indicate that an increase in carboxyl groups increases adsorption of all three groups of DBP precursors. Zhang et al. (2015) postulated a link between chemical and physical CNT characteristics that may be relevant here: repulsive forces created by negatively charged oxygen-containing functional groups enlarge spaces between individual CNTs in bundles thereby increasing CPV and S_{BET}. Additionally, functional groups generally form at defect sites in the CNT walls which are also locations that

allow access inner microporosity or mesoporosity (depending on the inner diameter of the CNT) (Yang et al., 2005). It has also been shown that the presence of surface oxides increases the hydrophilicity of CNT surfaces, which could enhance the adsorption of hydrophilic DBP precursors, such as those that react with chloramines to form *N*-nitrosamines (Zhang et al., 2015). Additionally, amine-based groups serving as *N*-nitrosamine precursors are positively charged at circumneutral pH. Thus, these groups would experience electrostatic attractions to the negatively charged carboxylic acid functionalities on the CNTs, which may explain the high removal of TONO precursors relative to TTHM and DHAN precursors. Hydrogen bonding may also be an important adsorption mechanism, which would be consistent with our results, as increases in oxygen groups will increase adsorption when hydrogen bonding is important (Pan and Xing, 2008). However, application of CNTs in the water produces hydrophobic interactions that could obscure the contribution of hydrogen bonding as an adsorption mechanism. The multicollinearity of the physical and chemical properties indicates that both CPV and oxygen-containing functional groups are important to CNT performance for DBP precursor removal.

To explore the concept of DBP precursor size exclusion from the CNT pore networks, linear regression models were refit for all DBP types by arbitrarily increasing minimum pore widths used for the computation of pore volume while all other variables remained unchanged (Figure 3). For TTHM, CPV p-values were large ($p > 0.5$) at low pore widths (< 5 nm) and only came close to significance ($p = 0.079$) above 15 nm. For DHAN, CPV p-values decreased from ~0.15 and became significant ($p = 0.05$) near a minimum pore width of 7 nm and remained significant throughout. For TONOFP, pore volume had a negative effect (i.e. more precursor adsorption occurred as pore volume increased) and pore width had relatively little impact on the importance of pore volume. On balance, the results in Figure 3 indicate that size exclusion

effects by the CNT pores could impact adsorption of TTHM and DHAN precursors, but not TONO precursors. The trends in Figure 3 could indicate that TONO precursors are generally smaller in size (or more accessible to the smaller CNT pores) than TTHM and DHAN precursors. At smaller pore widths, TONO precursors may not have much competition for adsorption sites; as pore width increases toward pores in excess of 15 nm, larger and more abundant TTHM and DHAN precursors could utilize a greater portion of the adsorption capacity. Others have shown that larger molecules at relatively high concentrations (such as TTHM precursors) can block CNT pores and limit further adsorption, while small molecules at trace concentrations (such as TONO precursors) experience little competition for adsorption sites (Hanigan et al., 2015).

3.4. Fluorescence Metrics as DBP Precursor Surrogates

Fluorescence EEMs were measured on untreated and CNT-treated (but not chloraminated) waters to evaluate its usefulness as a precursor surrogate and perhaps limit time-consuming DBPFP analyses in upcoming studies. Fluorescence intensities at all wavelength pairs measured were regressed against the DBP data to identify pairs for which strong correlations exist. Figure 4 shows the correlation coefficients presented on axes equivalent to the EEMs for TTHMFP (Panel A, $R_{MAX}^2 = 0.86$), DHANFP (Panel B, $R_{MAX}^2 = 0.88$), and TONOFP (Panel C, $R_{MAX}^2 = 0.50$) in WS-EFF, and TTHMFP (Panel D, $R_{MAX}^2 = 0.78$) and DHANFP (Panel E, $R_{MAX}^2 = 0.80$) in BL-RAW. These correlations represent relationships between DBP precursors remaining after treatment with CNTs and DBP concentrations formed following FP tests, performed using a recently developed method (Do et al., 2015). As expected, correlations are strong for TTHMFP and DHANFP in both waters. However, the moderate correlation coefficients for TONOFP indicate that fluorescence is unlikely to be a suitable precursor

surrogate for total *N*-nitrosamine precursor concentrations when applied in this manner. Interestingly, samples from WS-EFF (Figures 4A, 4B, and 4C) show a large region of wavelength pairs that give high correlation coefficients. In contrast, high R_{MAX}^2 values for BL-RAW (Figures 4D and 4E) are more localized and are centered near $I_{275/480}$. The insensitivity in R^2 values shown in Figures 4A, 4B, and 4C was unexpected in light of several studies attributing the various regions of EEMs to distinct fluorophore groups (i.e., humic-, fulvic-, tryptophan-, and tyrosine-like), each with its unique chemistry (Hudson et al., 2007). The results presented in Figure 4 suggest strong relationships among virtually all wavelength pairs, and thus imply interdependence (i.e. an increase in a particular fluorophore group could impact other regions of the EEM). Fluorescence EEMs were also analyzed by PARAFAC analysis. A detailed discussion of the removal of the PARAFAC components by the CNTs and correlations between PARAFAC components (Table S5) is provided in the SI. This analysis advances our assertion of fluorophore interdependence, which prevents valid conclusions regarding the affinity of CNTs for discrete humic-, fulvic- and protein-like fluorophores. The interdependence observed in both EEM correlations and PARAFAC components may be indicative of interferences on the protein-like fluorophores and preclude the use of fluorescence EEMs alone as a surrogate for TONO precursors. However, the nature of these precursors suggests that fluorescence may be utilized following elimination of interfering humics (Wang et al., 2015), in applications such as asymmetric flow field-flow fractionation where proteins can be physically separated from humics prior to fluorescence measurements.

3.5. Implications

Based on the importance of surface oxides and CPV for DBP precursor removal, future studies are needed to enhance these CNT characteristics and test their impact in sorption

systems. Oxidative treatment with a mixture of nitric and sulfuric acid has been shown to result in formation of oxygen-containing groups on SWCNTs (Balasubramanian and Burghard, 2005; Komarova et al., 2015) and MWCNTs (Ago et al., 1999). Additionally, KOH treatment can increase surface area and pore volume, specifically in mesopores (Niu et al., 2007). Based on the size exclusion results (Figure 3), this may be particularly important to improve sorption of DHAN and TTHM precursors. Furthermore, future studies of CNT modification should be paired with a reliable system for CNT integration into DWTP treatment processes. A large range of possibilities now exists regarding design of freeform CNT microstructures grown on substrates that could be adapted into current treatment processes. These microstructures can be grown to exacting specifications of size, shape, and porosity, and conformal coating can be applied to manipulate chemical properties (De Volder et al., 2014). Additionally, incorporation of CNTs into hollow fiber membranes has been shown to increase membrane flux, fouling resistance, thermal stability, porosity, and electrochemically regenerative capability with minimal CNT leaching (Huang et al., 2014; Wei et al., 2014; Jafari et al., 2015).

4. Conclusions

With no modification, CNTs have natural affinity for THM-, DHAN, and TONO precursors. The breadth of applications discovered for CNTs due to their unique set of physiochemical properties speak to their potential for further commercial availability. Though CNTs are a novel sorbent with higher costs than standard sorbents, higher performance levels – particularly with regard to TONO precursor adsorption – give CNTs an advantage that warrants future study. As production costs decrease and the body of research regarding their applications increases, CNTs gain potential for feasibility of application in conventional water treatment systems. Manipulation of physicochemical properties to enhance DBP precursor adsorption in

concert with reliable methods of integration into water treatment processes could provide DWTPs with a new technique for meeting the increasingly rigorous water quality standards for DBP control.

4. Figures and Tables

Table 1. Physical and Chemical Characteristics of the selected CNTs

CNT Type	Physical Characteristics from SAA[1]		Relative Amount of Chemical Bonds from XPS[2]			
	CPV[3] ($cm^3\ g^{-1}$)	S_{BET}[4] ($m^2\ g^{-1}$)	C=C or C-C[5]	C-O[6]	C=O[7]	COO[8]
1	0.598	446	77.75	8.56	2.70	1.83
2	1.267	837	73.83	10.25	2.90	1.09
3	0.163	104	78.55	7.07	2.98	1.45
4	0.627	426	75.09	8.53	3.90	2.23
5	0.296	171	76.89	7.86	2.65	2.11
6	0.541	298	78.17	7.72	2.88	1.73
7	0.135	92	80.85	6.76	1.81	1.97
8	0.442	265	78.40	7.80	2.18	1.98
9	0.471	262	77.13	7.45	3.00	1.91

[1]Quantachrome Nova 2200e Surface Area and Pore Size Analyzer;
[2]PHI 5000 VersaProbe x-ray photoelectron spectrometer, reported as the percent of total carbon bond types present and does not include shake-up features
[3]Cumulative Pore Volume;
[4]Surface area calculated using the Brunauer-Emmett-Teller (BET) model; [5]Analyzed as total of C=C, C-C, and C-H bonds;
[6]Alcohol bonds;
[7]Carbonyl bonds;
[8]Carboxyl bonds

Table 2. Linear regression models of DBP ratio for TTHMFP, DHANFP and TONOFP

Independent Variables[1]	TTHMFP Ratio		DHANFP Ratio		TONOFP Ratio	
	Coeff.[2]	p-value	Coeff.	p-value	Coeff.	p-value
DOC Ratio	0.618*	0.000	0.427*	0.005	1.667	0.097
UV_{254} Ratio	0.039	0.731	0.384*	0.003	-1.900**	0.016
Water Type[3]	-0.099**	0.000	0.050*	0.009	-	-
CNT Dose (mg/L)	-0.004**	0.000	-0.003**	0.006	-0.011**	0.001
Carbon-Carbon Bonds (%)	0.018	0.441	0.002	0.918	-0.014	0.823
Alcohol Groups (%)	0.028	0.682	-0.081	0.264	0.445*	0.016
Carbonyl Groups (%)	-0.007	0.859	0.026	0.537	-0.089	0.462
Carboxyl Groups (%)	-0.112**	0.002	-0.212**	0.000	-0.246**	0.010
BET Surface Area ($m^2\ g^{-1}$)	-0.000	0.837	0.001	0.239	0.000	0.798
CPV[4] ($mL\ g^{-1}$)	-0.096	0.679	-0.376	0.140	-2.246**	0.001
Constant	-1.034	0.666	0.919	0.710	-0.042	0.994

*Positive significance ($p < 0.05$)

**Negative significance ($p < 0.05$)

[1]Independent variables all represent terms in regression equations

[2]Regression coefficients

[3]Binary variable distinguishing between BL-RAW and WS-EFF samples, not applicable to TONO ratio

[4]Cumulative Pore Volume.

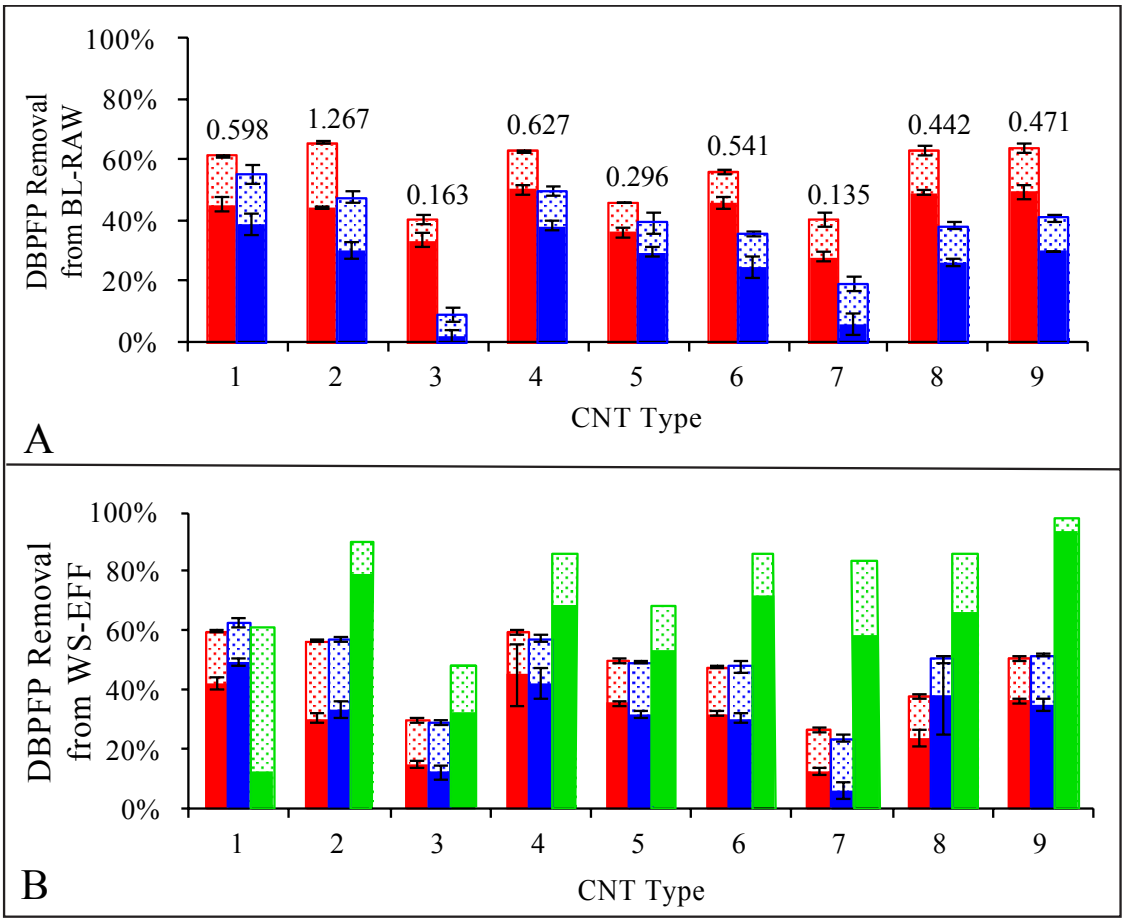

Figure 1. Percent removal of TTHMFP (■ 25 mg•L^{-1} CNT dose, □ 50 mg•L^{-1} CNT dose), DHANFP (■ 25 mg•L^{-1} CNT dose, □ 50 mg•L^{-1} CNT dose) and TONOFP (■25 mg•L^{-1} CNT dose, □ 50 mg•L^{-1} CNT dose) by nine CNT types from Beaver Lake raw water (BL-RAW, Figure 1A) and West Side wastewater treatment plant effluent (WS-EFF, Figure 1B). Values above bars in Figure 1A correspond to the CPV (cm^3•g^{-1}) of each CNT Type and hold true in Figure 1B as well. For TTHMFP and DHANFP, 95% confidence intervals are shown based on triplicate samples on a molar basis. Average FP for untreated BL-RAW samples was 0.095- and 0.022 µmol•L^{-1} for TTHMs and DHANs respectively and 0.250- and 0.086 µmol•L^{-1} respectively in WS-EFF. TONOFP was measured for WS-EFF only in mass-based units as NDMA with an average concentration of 400 ng•L^{-1} as NDMA for untreated samples.

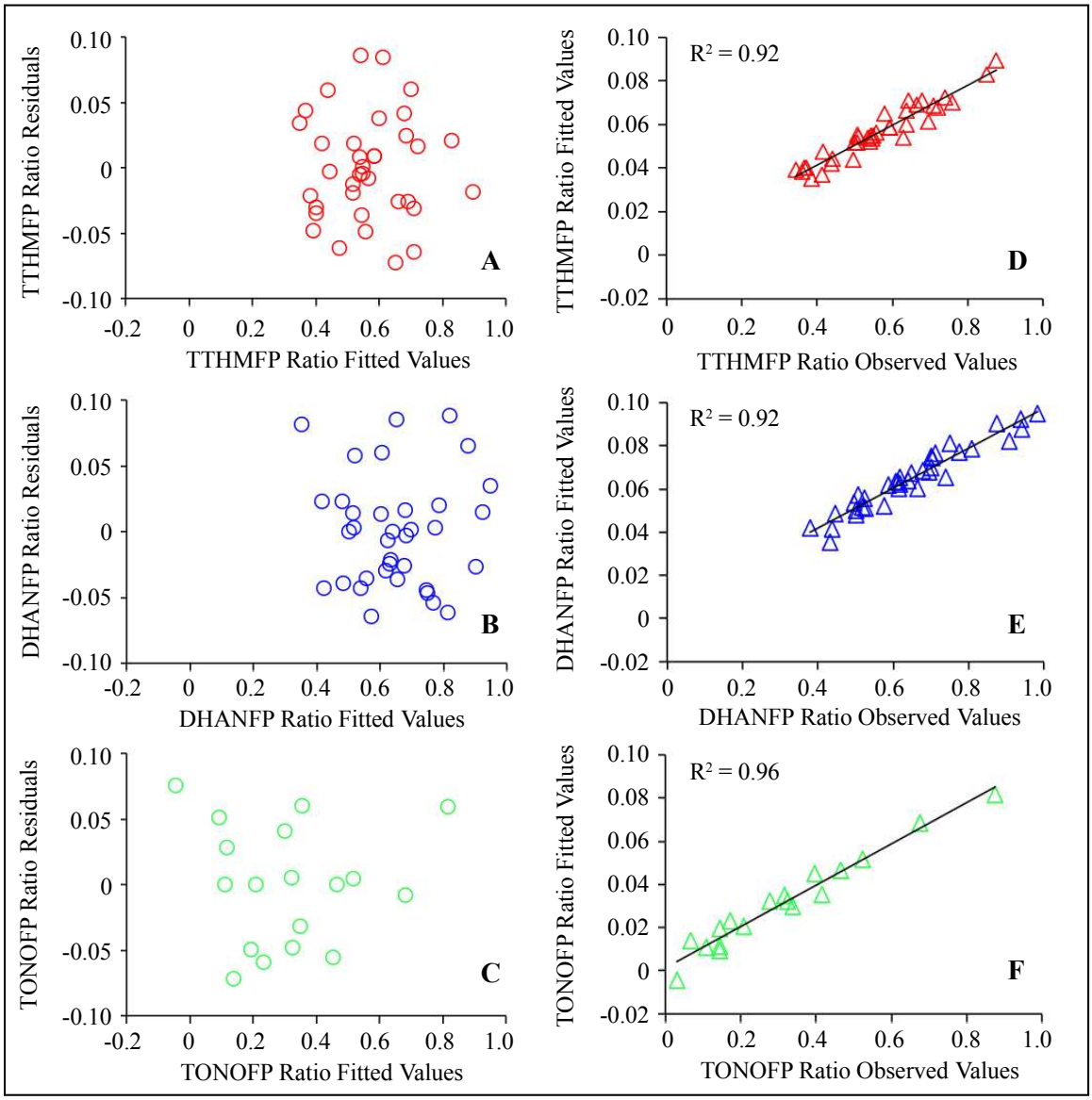

Figure 2. Error variance of models for TTHMFP Ratio (Figure 2A), DHANFP Ratio (Figure 2B) and TONOFP (Figure 2C) and representations of model correlations with observed values of TTHMFP, DHANFP and TONOFP Ratios (Figures 2D-2F). Independent variables used to fit models of TTHMFP, DHANFP, and TONOFP Ratio are detailed in Table 2.

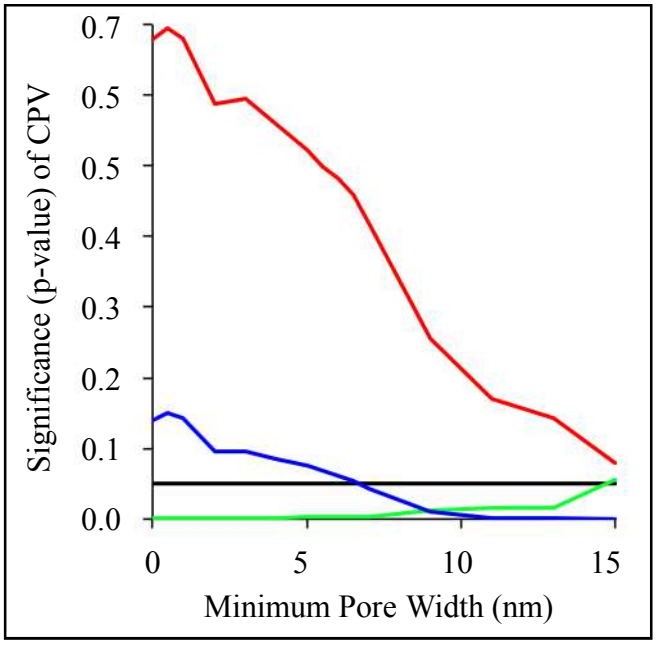

Figure 3. Significance of Cumulative Pore Volume (CPV) in linear regression models (see Table 2) of TTHMFP ratio (–), DHANFP ratio (–) and TONOFP ratio (–) as calculated by arbitrarily increasing the minimum pore widths used to calculate CPV for all nine types of carbon nanotubes. A p-value of 0.05 is included to illustrate the point below which CPV is statistically significant.

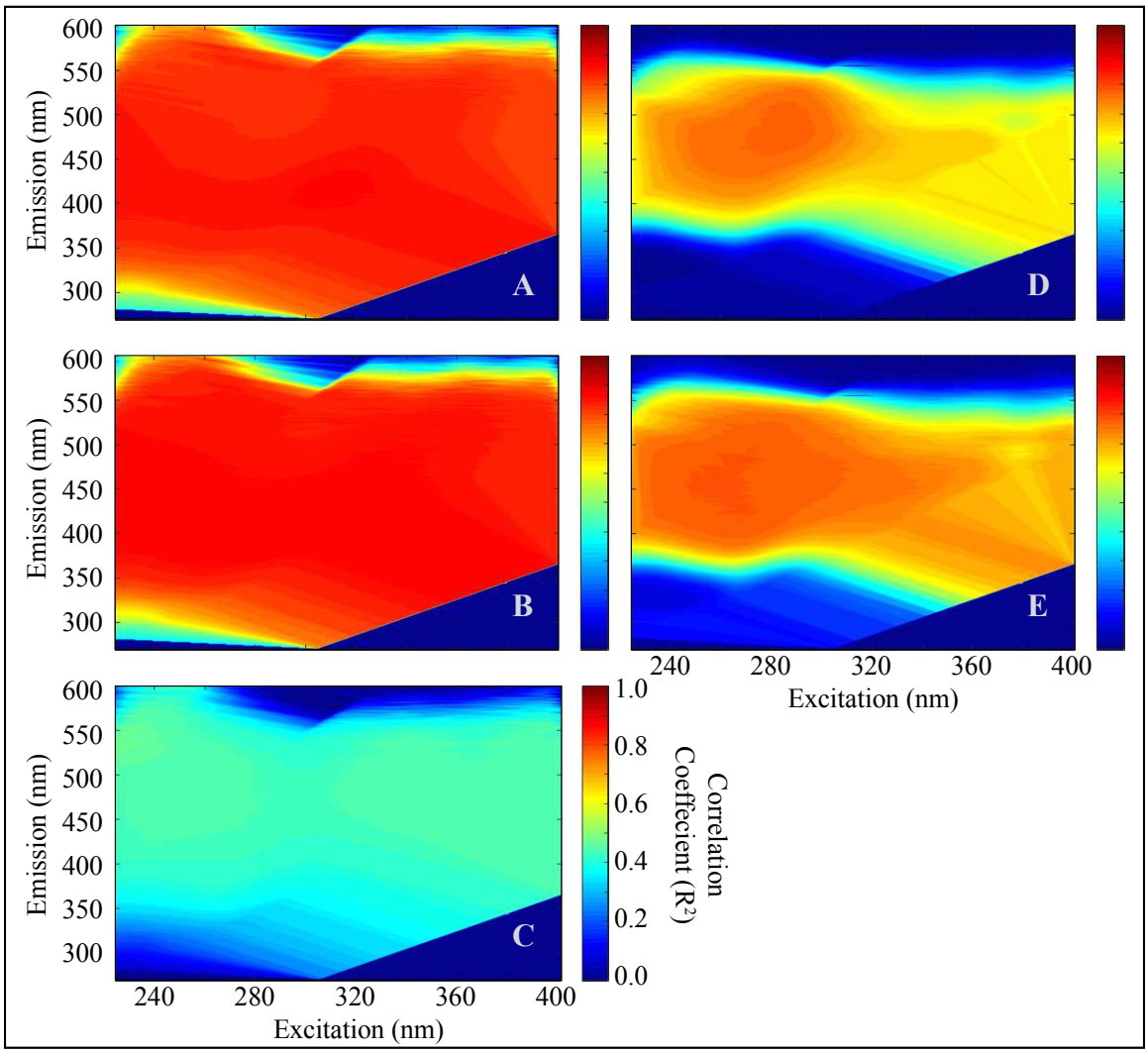

Figure 4. Correlation coefficients for fluorescence intensities of WS-EFF samples in relation to TTHMFP (Figure 4A), DHANFP (Figure 4B) and TONOFP (Figure 4C) and of BL-RAW samples in relation to TTHMFP (Figure 4D) and DHANFP (Figure 4E).

5. References

Adeniran, B. and Mokaya, R., 2015. Low temperature synthesized carbon nanotube superstructures with superior CO2 and hydrogen storage capacity. Journal of Materials Chemistry A 3 (9), 5148-5161.

Ago, H., Kugler, T., Cacialli, F., Salaneck, W. R., Shaffer, M. S. P., Windle, A. H. and Friend, R. H., 1999. Work functions and surface functional groups of multiwall carbon nanotubes. Journal of Physical Chemistry B 103 (38), 8116-8121.

Andersen, C. M. and Bro, R., 2003. Practical aspects of PARAFAC modeling of fluorescence excitation-emission data. Journal of Chemometrics 17 (4), 200-215.

Apul, O. G. and Karanfil, T., 2015. Adsorption of synthetic organic contaminants by carbon nanotubes: A critical review. Water Research 68, 34-55.

Balasubramanian, K. and Burghard, M., 2005. Chemically functionalized carbon nanotubes. Small 1 (2), 180-192.

Birch, M. E., Ruda-Eberenz, T. A., Chai, M., Andrews, R. and Hatfield, R. L., 2013. Properties that influence the specific surface areas of carbon nanotubes and nanofibers. Annals of Occupational Hygiene 57 (9), 1148-1166.

Cho, H.-H., Smith, B. A., Wnuk, J. D., Fairbrother, D. H. and Ball, W. P., 2008. Influence of surface oxides on the adsorption of naphthalene onto multiwalled carbon nanotubes. Environmental Science & Technology 42 (8), 2899-2905.

Cory, R. M., Miller, M. P., McKnight, D. M., Guerard, J. J. and Miller, P. L., 2010. Effect of instrument-specific response on the analysis of fulvic acid fluorescence spectra. Limnology and Oceanography-Methods 8, 67-78.

Dai, N. and Mitch, W. A., 2013. Relative importance of N-nitrosodimethylamine compared to total N-nitrosamines in drinking waters. Environmental Science & Technology 47 (8), 3648-3656.

Dai, N., Shah, A. D., Hu, L. H., Plewa, M. J., McKague, B. and Mitch, W. A., 2012. Measurement of Nitrosamine and Nitramine Formation from NO Reactions with Amines during Amine-Based Carbon Dioxide Capture for Postcombustion Carbon Sequestration. Environmental Science & Technology 46 (17), 9793-9801.

Das, R., Hamid, S. B. A., Ali, M. E., Ismail, A. F., Annuar, M. S. M. and Ramakrishna, S., 2014. Multifunctional carbon nanotubes in water treatment: The present, past and future. Desalination 354, 160-179.

De Volder, M., Park, S., Tawfick, S. and Hart, A. J., 2014. Strain-engineered manufacturing of freeform carbon nanotube microstructures. Nature Communications 5.

Devore, J. L., 2004. Probability and statistics for engineering and the sciences, 6, Brooks/Cole, Thomson Learning, Belmont, CA.

Do, T. D., Chimka, J. R. and Fairey, J. L., 2015. Improved (and singular) disinfectant protocol for indirectly assessing organic precursor concentrations of trihalomethanes and dihaloacetonitriles. Environmental Science & Technology 49 (16), 9858-9865.

Draper, N. R. and Smith, H., 1998. Applied regression analysis, John Wiley & Sons, Inc., New York.

Eaton, A. D., Clesceri, L.S., Rice, E.W., Greenberg, A.E. (Eds.) (2005). Standard methods for the examination of water & wastewater, American Public Health Association, Washington, DC.

Hanigan, D., Zhang, J., Herckes, P., Krasner, S. W., Chen, C. and Westerhoff, P., 2012. Adsorption of N-nitrosodimethylamine precursors by powdered and granular activated carbon. Environmental Science & Technology 46 (22), 12630-12639.

Hanigan, D., Zhang, J., Herckes, P., Zhu, E., Krasner, S. and Westerhoff, P., 2015. Contribution and removal of watershed and cationic polymer N-nitrosodimethylamine precursors. Journal American Water Works Association 107 (3), 90-91.

Hrudey, S. E. and Charrois, J. W. A., Eds. (2012). Disinfection by-products and human health. IWA Publishing and Australian Water Association, London.

Huang, H., Fairbrother, H., Teychene, B., Ajmani, G., Chalew, T. A., Gallagher, M. J., Cho, H., Schwab, K. and Jacangelo, J., 2014. Carbon nanotube composite membranes for small 'designer' water treatment systems. Water Science and Technology-Water Supply 14 (5), 917-923.

Hudson, N., Baker, A. and Reynolds, D., 2007. Fluorescence analysis of dissolved organic matter in natural, waste and polluted waters - A review. River Research and Applications 23 (6), 631-649.

Iriarte-Velasco, U., Alvarez-Uriarte, J. I., Chimeno-Alanis, N. and Gonzalez-Velasco, J. R., 2008. Natural Organic Matter Adsorption onto Granular Activated Carbons: Implications in the Molecular Weight and Disinfection Byproducts Formation. Industrial & Engineering Chemistry Research 47 (20), 7868-7876.

Jafari, A., Mahvi, A. H., Nasseri, S., Rashidi, A., Nabizadeh, R. and Rezaee, R., 2015. Ultrafiltration of natural organic matter from water by vertically aligned carbon nanotube membrane. Journal of Environmental Health Science and Engineering 13, 51.

Karanfil, T., Cheng, W., Dastgheib, S., Guo, Y. and Song, H., 2007. DBP formation control by modified activated carbons, Awwa Research Foundation Denver, CO.

Karanfil, T., Erdogan, I. and Schlautman, M. A., 2003. Selecting filter membranes for measuring DOC and UV_{254}. Journal American Water Works Association 95 (3), 86-100.

Komarova, N. y. S., Krivenko, A. G., Ryabenko, A. G., Naumkin, A. V., Maslakov, K. I. and Savilov, S. V., 2015. Functionalization and defunctionalization of single walled carbon nanotubes: Electrochemical and morphologic consequences. Journal of Electroanalytical Chemistry 738, 27-34.

Kovtyukhova, N. I., Mallouk, T. E., Pan, L. and Dickey, E. C., 2003. Individual single-walled nanotubes and hydrogels made by oxidative exfoliation of carbon nanotube ropes. Journal of the American Chemical Society 125 (32), 9761-9769.

Krasner, S. W., Mitch, W. A., McCurry, D. L., Hanigan, D. and Westerhoff, P., 2013. Formation, precursors, control, and occurrence of nitrosamines in drinking water: A review. Water Research 47 (13), 4433-4450.

Krasner, S. W., Weinberg, H. S., Richardson, S. D., Pastor, S. J., Chinn, R., Sclimenti, M. J., Onstad, G. D. and Thruston, A. D., 2006. Occurrence of a new generation of disinfection byproducts. Environmental Science & Technology 40 (23), 7175-7185.

Kristiana, I., Lethorn, A., Joll, C. and Heitz, A., 2014. To add or not to add: The use of quenching agents for the analysis of disinfection by-products in water samples. Water Research 59, 90-98.

Kulshrestha, P., McKinstry, K. C., Fernandez, B. O., Feelisch, M. and Mitch, W. A., 2010. Application of an optimized total N-nitrosamine (TONO) assay to pools: placing N-nitrosodimethylamine (NDMA) determinations into perspective. Environmental Science & Technology 44 (9), 3369-3375.

Kundu, S., Xia, W., Busser, W., Becker, M., Schmidt, D. A., Havenith, M. and Muhler, M., 2010. The formation of nitrogen-containing functional groups on carbon nanotube surfaces: a quantitative XPS and TPD study. Physical Chemistry Chemical Physics 12 (17), 4351-4359.

Liao, X. B., Wang, C. K., Wang, J., Zhang, X. J., Chen, C., Krasner, S. W. and Suffet, I. H., 2014. Nitrosamine precursor and DOM control in effluent-affected drinking water. Journal American Water Works Association 106 (7), 81-82.

Liu, Y., Zhao, Y., Sun, B. and Chen, C., 2013. Understanding the toxicity of carbon nanotubes. Accounts of Chemical Research 46 (3), 702-713.

Lu, C. Y. and Su, F. S., 2007. Adsorption of natural organic matter by carbon nanotubes. Separation and Purification Technology 58 (1), 113-121.

Mayer, L. M., Schick, L. L. and Loder, T. C., 1999. Dissolved protein fluorescence in two Maine estuaries. Marine Chemistry 64 (3), 171-179.

McKnight, D. M., Boyer, E. W., Westerhoff, P. K., Doran, P. T., Kulbe, T. and Andersen, D. T., 2001. Spectrofluorometric characterization of dissolved organic matter for indication of precursor organic material and aromaticity. Limnology and Oceanography 46 (1), 38-48.

McPhail, M. R., Sells, J. A., He, Z. and Chusuei, C. C., 2009. Charging nanowalls: adjusting the carbon nanotube isoelectric point via surface functionalization. Journal of Physical Chemistry C 113 (32), 14102-14109.

Mitch, W. A. and Dai, N. (2012). Water Research Foundation Report #4209: Development and application of a total nitrosamine assay for disinfected waters, Water Research Foundation.

Najm, I. N., Snoeyink, V. L., Lykins, B. W. and Adams, J. Q., 1991. USING POWDERED ACTIVATED CARBON - A CRITICAL-REVIEW. Journal American Water Works Association 83 (1), 65-76.

Niu, J. J., Wang, J. N., Jiang, Y., Su, L. F. and Ma, J., 2007. An approach to carbon nanotubes with high surface area and large pore volume. Microporous and Mesoporous Materials 100 (1-3), 1-5.

Okpalugo, T. I. T., Papakonstantinou, P., Murphy, H., McLaughlin, J. and Brown, N. M. D., 2005. High resolution XPS characterization of chemical functionalised MWCNTs and SWCNTs. Carbon 43 (1), 153-161.

Pan, B. and Xing, B., 2008. Adsorption mechanisms of organic chemicals on carbon nanotubes. Environmental Science & Technology 42 (24), 9005-9013.

Pehlivanoglu-Mantas, E. and Sedlak, D. L., 2008. Measurement of dissolved organic nitrogen forms in wastewater effluents: Concentrations, size distribution and NDMA formation potential. Water Research 42 (14), 3890-3898.

Pifer, A. D. and Fairey, J. L., 2012. Improving on $SUVA_{254}$ using fluorescence-PARAFAC analysis and asymmetric flow-field flow fractionation for assessing disinfection byproduct formation and control. Water Research 46 (9), 2927-2936.

Pifer, A. D. and Fairey, J. L., 2014. Suitability of organic matter surrogates to predict trihalomethane formation in drinking water sources. Environmental Engineering Science 31 (3), 117-126.

Ramanathan, T., Fisher, F. T., Ruoff, R. S. and Brinson, L. C., 2005. Amino-functionalized carbon nanotubes for binding to polymers and biological systems. Chemistry of Materials 17 (6), 1290-1295.

Ren, X., Chen, C., Nagatsu, M. and Wang, X., 2011. Carbon nanotubes as adsorbents in environmental pollution management: A review. Chemical Engineering Journal 170 (2-3), 395-410.

Rook, J. J., 1976. Haloforms in drinking water. Journal American Water Works Association 68 (3), 168-172.

Russell, C. G., Blute, N. K., Via, S., Wu, X. and Chowdhury, Z., 2012. National assessment of nitrosamine occurrence and trends. Journal American Water Works Association 104 (3), E205-E217.

Sen, S., Haggard, B. E., Chaubey, I., Brye, K. R., Costello, T. A. and Matlock, M. D., 2007. Sediment phosphorus release at Beaver Reservoir, Northwest Arkansas, USA, 2002-2003: A preliminary investigation. Water, Air and Soil Pollution 179 (1-4), 67-77.

Shah, A. D. and Mitch, W. A., 2012. Halonitroalkanes, Halonitriles, Haloamides, and N-Nitrosamines: A Critical Review of Nitrogenous Disinfection Byproduct Formation Pathways. Environmental Science & Technology 46 (1), 119-131.

Shapiro, S. S. and Wilk, M. B., 1965. An analysis of variance test for normality (complete samples). Biometrika 52, 591-611.

Shih, Y.-h. and Li, M.-S., 2008. Adsorption of selected volatile organic vapors on multiwall carbon nanotubes. Journal of Hazardous Materials 154 (1-3), 21-28.

Sing, K. S. W., Everett, D. H., Haul, R. A. W., Moscou, L., Pierotti, R. A., Rouquerol, J. and Siemieniewska, T., 1985. Reporting physisorption data for gas solid systems with special reference to the determination of surface area and porosity (recommendations 1984). Pure and Applied Chemistry 57 (4), 603-619.

Singh, B., Fang, Y., Cowie, B. C. C. and Thomsen, L., 2014. NEXAFS and XPS characterisation of carbon functional groups of fresh and aged biochars. Organic Geochemistry 77, 1-10.

StataCorp (2009). Stata statistical software: release 11. College Station, TX, StataCorp LP.

Stedmon, C. A. and Bro, R., 2008. Characterizing dissolved organic matter fluorescence with parallel factor analysis: a tutorial. Limnology and Oceanography-Methods 6, 572-579.

Tawfick, S., De Volder, M., Copic, D., Park, S. J., Oliver, C. R., Polsen, E. S., Roberts, M. J. and Hart, A. J., 2012. Engineering of micro- and nanostructured surfaces with anisotropic geometries and properties. Advanced Materials 24 (13), 1628-1674.

Upadhyayula, V. K. K., Deng, S., Mitchell, M. C. and Smith, G. B., 2009. Application of carbon nanotube technology for removal of contaminants in drinking water: A review. Science of the Total Environment 408 (1), 1-13.

Wang, C. K., Zhang, X. J., Wang, J., Liu, S. M., Chen, C. and Xie, Y. F., 2013. Effects of organic fractions on the formation and control of N-nitrosamine precursors during conventional drinking water treatment processes. Science of the Total Environment 449, 295-301.

Wang, H., Zhou, A., Peng, F., Yu, H. and Yang, J., 2007. Mechanism study on adsorption of acidified multiwalled carbon nanotubes to Pb(II). Journal of Colloid and Interface Science 316 (2), 277-283.

Wang, X., Tao, S. and Xing, B., 2009. Sorption and competition of aromatic compounds and humic acid on multiwalled carbon nanotubes. Environmental Science & Technology 43 (16), 6214-6219.

Wang, Z. G., Cao, J. and Meng, F. G., 2015. Interactions between protein-like and humic-like components in dissolved organic matter revealed by fluorescence quenching. Water Research 68, 404-413.

Wei, G., Yu, H., Quan, X., Chen, S., Zhao, H. and Fan, X., 2014. Constructing all carbon nanotube hollow fiber membranes with improved performance in separation and antifouling for water treatment. Environmental Science & Technology 48 (14), 8062-8068.

Yan Yan, H. and Terentjev, E. M., 2012. Dispersion of carbon nanotubes: mixing, sonication, stabilization, and composite properties. Polymers 4 (1), 275-95.

Yang, C. M., Kim, D. Y. and Lee, Y. H., 2005. Single-walled carbon nanotube network with bimodal pore structures of uniform microporosity and mesoporosity. Journal of Nanoscience and Nanotechnology 5 (6), 970-974.

Yang, K. and Xing, B., 2009. Adsorption of fulvic acid by carbon nanotubes from water. Environmental Pollution 157 (4), 1095-1100.

Zepp, R. G., Sheldon, W. M. and Moran, M. A., 2004. Dissolved organic fluorophores in southeastern US coastal waters: correction method for eliminating Rayleigh and Raman scattering peaks in excitation-emission matrices. Marine Chemistry 89 (1-4), 15-36.

Zhang, S., Shao, T., Kose, H. S. and Karanfil, T., 2010. Adsorption of aromatic compounds by carbonaceous adsorbents: a comparative study on granular activated carbon, activated carbon fiber, and carbon nanotubes. Environmental Science & Technology 44 (16), 6377-6383.

Zhang, Y., Chen, C., Peng, L., Ma, Z., Zhang, Y., Xia, H., Yang, A., Wang, L., Su, D. S. and Zhang, J., 2015. Carboxyl groups trigger the activity of carbon nanotube catalysts for the oxygen reduction reaction and agar conversion. Nano Research 8 (2), 502-511.

Zhang, Z., Pfefferle, L. and Haller, G. L., 2014. Comparing characterization of functionalized multi-walled carbon nanotubes by potentiometric proton titration, NEXAFS, and XPS. Chinese Journal of Catalysis 35 (6), 856-863.

Zhu, Y. W., Murali, S., Stoller, M. D., Ganesh, K. J., Cai, W. W., Ferreira, P. J., Pirkle, A., Wallace, R. M., Cychosz, K. A., Thommes, M., Su, D., Stach, E. A. and Ruoff, R. S., 2011. Carbon-based supercapacitors produced by activation of graphene. Science 332 (6037), 1537-1541.

Appendix 1

Supplementary Information for

"Trihalomethane, Dihaloacetonitrile, and Total *N*-nitrosamine Precursor Adsorption by Carbon Nanotubes: The Importance of Surface Oxides and Pore Volume"

List of Tables and Figures

Methods

Dissolved organic carbon was measured for each filtered sample using a GE 5310C TOC analyzer. Anion concentrations were measured for both BL-RAW and WS-EFF raw waters using a Metrohm 850 Ion Chromatograph with conductivity and UV detectors. Fluorescence EEMs were collected using a dual monochromator fluorescence detector (Agilent Technologies, Model G1321A). Wavelengths used were 250 to 400 nm for excitation and 270 to 600 nm for emission, both in 1 nm increments. A five-point standard curve of quinine sulfate in 0.1 M sulfuric acid was used due to its distinct response at excitation and emission wavelengths of 350 and 450 nm, respectively, and intensity measurements of all spectra were reported in quinine sulfate equivalents (Cory et al., 2010). Absorbance scans were used to correct for inner-filter effects as suggested by McKnight et al. (2001) and the MATLAB program *Cleanscan* (Zepp et al., 2004) was used to correct EEMs for Raleigh and Raman scattering. Values of fluorescence intensity at excitation and emission wavelengths of 345 nm and 425 nm, respectively, are strongly correlated with TTHM precursors (Do et al., 2015) and are shown in Table S1 for both BL-RAW and WS-EFF. Two models were developed using parallel factor (PARAFAC) analysis on arrays of EEMs for each water type to reveal components with distinct excitation-emission signatures and their maximum intensities, F_{MAX} (Andersen and Bro, 2003).

Disinfection by-product formation potential (DBPFP) of the samples was measured using the procedure detailed in Do et al. (2015) Samples were warmed to room temperature, amended with 20 mM sodium bicarbonate, and adjusted to pH 7.0 using NaOH and/or HCl. Pre-formed 14 $g \cdot L^{-1}$ as Cl_2 stock monochloramine solution was prepared immediately before chloramination as detailed previously. The stock total chlorine and monochloramine concentrations were measured on a representative sample volume, following 4,000-6,000 times dilution with Milli-Q water,

using Hach powder pillows with a UV-Vis 2450 spectrophotometer (Shimadzu) at wavelengths of 655- and 552 nm, respectively. Samples were dosed with pre-formed monochloramine at 300 $mg \cdot L^{-1}$ as Cl_2 and stored headspace-free in 1-L chlorine demand free amber glass bottles for 7 days in the dark at room temperature (25 ºC ± 2 ºC). Following the hold time, the monochloramine and total chlorine residuals were measured and quenched with 20.1 g of a salt mixture (mass ratio of 0.9 g ascorbic acid ($C_6H_8O_6$): 1 g KH_2PO_4: 39 g Na_2HPO_4) added to each 1 L sample to halt DBP formation reactions as recommended by Kristiana et al. (2014). Total trihalomethanes (TTHMs) and dihaloacetonitriles (DHANs) in the West Side wastewater treatment plant effluent (WS-EFF) samples were quantified by GC-ECD using a 9-point standard curve that ranged from 1- to 100 $\mu g \cdot L^{-1}$. Similarly, TTHMs and DHANs in the Beaver Lake raw water (BL-RAW) samples were analyzed using a 12-point standard curve that ranged from 0.1- to 100 $\mu g \cdot L^{-1}$. Blanks and check standards were run after every group of six samples.

The pH point of zero charge of the carbon nanotubes (CNTs) was not measured because a stable suspension could not be achieved without CNT modification. Sonication of CNTs in pure water was attempted despite the high probability of damage to the CNT structure (Yan Yan and Terentjev, 2012), but failed to produce the stable suspension necessary for zeta potential measurements.

PARAFAC Analysis

EEMs were analyzed by PARAFAC to further characterize the dissolved organic matter and help generalize the precursor surrogate findings. Given the differences in the water types, separate PARAFAC models were used for BL-RAW and WS-EFF samples, each originally consisting of 57 EEMs. Two outliers were removed from the BL-RAW data set while no outliers were found in WS-EFF samples. Split-half analyses showed that BL-RAW samples could be adequately described by a two- or four-component model and the WS-EFF samples could be described by a two- or three-component model. Models with the greatest number of components (i.e., four components for BL-RAW and three components for WS-EFF) were chosen to explain the data because they had the smallest sum of squared errors (Figure S8).

XPS Data Analysis

Binding energy scales were charge corrected using a C1s peak position of 284.4 eV (Ago et al., 1999; McPhail et al., 2009). C1s peaks were deconvoluted with a Gaussian-Lorentzian mix function, allowed to range from 70-80% Gaussian distribution, and a Shirley background subtraction (McPhail et al., 2009; Zhang et al., 2014). An asymmetry parameter of 0.19 was applied to the peak representing carbon-carbon bonds (Ago et al., 1999); other bonds assigned were alcohols (C-O), carbonyls (C=O), and carboxyls (COO) with an additional peak fitted to the shake-up features satellite located in the higher binding energy region. Peak locations chosen for the carbon spectra deconvolutions were set as allowable ranges based on ranges found in the literature. Actual peak locations were allowed to vary within the set range in order to achieve the best fit determined by the chi-squared value of the model. The assymetric carbon peak representing all types of carbon-carbon bonding was set to 284.38-285.50 eV (Ago et al., 1999; Kovtyukhova et al., 2003; Okpalugo et al., 2005; Wang et al., 2007; Zhang et al., 2014).

Locations of various types of carbon-oxygen bonds are as follows: alcohol at 286.00-287.53 eV, carbonyl at 286.45-288.03 eV, and carboxyl at 288.39-289.55 eV (Ago et al., 1999; Kovtyukhova et al., 2003; Okpalugo et al., 2005; Ramanathan et al., 2005; Wang et al., 2007; McPhail et al., 2009; Singh et al., 2014). Shake-up features associated with π-π^* transitions were fitted at 289.00-291.60 eV (Okpalugo et al., 2005). Each individual peak was allowed to vary from 70- to 80% Gaussian distribution in order to find the best fit (McPhail et al., 2009; Kundu et al., 2010; Zhang et al., 2014).

Model Verification and Permutations

Results in Table 2 are based on reasonable assumptions with respect to a normal distribution of residuals and constant error variance. The results of the Wilk-Shapiro test (Shapiro and Wilk, 1965) for TTHM ($p = 0.788$), DHAN ($p = 0.066$) and TONO ($p = 0.339$) were all greater than $p = 0.05$; we therefore fail to reject a normal distribution of residuals.

Further investigation of the relationships between physical and chemical characteristics of the nine CNT types through simple linear regressions revealed strong correlations between percent alcohol groups and S_{BET} ($R^2 = 0.95$) and CPV ($R^2 = 0.90$). Multiple linear regression models of surface oxide groups and physical characteristics showed that alcohol groups were significant to S_{BET} and CPV when controlling for carbonyl and carboxyl groups. These findings show that multicollinearity of alcohol groups and physical properties results in variance inflation factors ($VIF = (1 - R^2)^{-1}$, where R^2 is relevant to a multiple linear regression model of one independent variable versus the other independent variables) greater than ten, which could make it impossible to observe otherwise significant independent variables in models of DBP ratio. Of the physical and chemical characteristics, carboxyl groups suffer least from variance inflation ($VIF = 1.27$), and it is possible that this variable serves as a surrogate for significance of physical

characteristics. To further study possible significance of alcohol groups in the face of multicollinearity, the carbonyl groups variable, which was insignificant in all models, was deleted from models of TTHM and DHAN Ratios. This deletion revealed negative significance of alcohol groups to DHAN ratio, indicating that an increase in alcohol groups improved removal of DHAN precursors.

As further evidence of multicollinearity, linear regression between S_{BET} and CPV variables also results in a very strong correlation ($R^2 = 0.97$). However, in the multivariate analysis including both physical variables, only CPV was significant to changes in DBPFP Ratio when controlling for surface area. The same cannot be said of S_{BET} when controlling for CPV. As the multivariate model is capable of providing a more comprehensive assessment of the significance of variables than simple linear regression of variable pairs, it is reasonable to conclude that CPV is a more relevant variable to discuss than S_{BET} in terms of relationships to chemical characteristics and DBPFP Ratio.

Nevertheless, Figure S4 shows the linear regressions for the wavelength pair associated with the maximum R^2 value for TTHM ($I_{369/365}$) and DHAN ($I_{379/356}$). Samples were included regardless of DBP type (TTHM and DHAN only) or source water and an aggregate R^2 value of 0.91 indicates that fluorescence measurements can be used as a reliable surrogate of organic precursor concentrations for TTHM and DHAN. As detailed in the SI, UV_{254} was also assessed as a DBP surrogate, but lacked sensitivity at low absorbance values (less than 0.05 cm^{-1}).

Modeling CNT Wall Type

Of the nine types of CNTs studied, two are single-walled (SWCNTs) and seven are multi-walled (MWCNTs). To explore the effects of these designations, a binary variable was added to the model to distinguish between SWCNTs and MWCNTs in addition to their physical

and chemical characteristics (Table 1). This binary variable was significant in both TTHM and DHAN models and showed that DBP ratios were significantly smaller in SWCNT-treated waters (i.e., SWCNTs adsorbed more TTHM and DHAN precursors). Also, controlling for the new binary variable, CPV had negative, significant effects on DBP ratio for DHAN in general (n = 36) and for TTHM in WS-EFF only (n = 18). However, without more observations of SWCNT types and/or greater chemical and physical detail to distinguish between single- and multi-walled CNTs, this study does not focus on the general difference in CNT wall type and its relationship to other variables.

Removal of PARAFAC Components

The maxima locations of PARAFAC Components 1 and 3 in BL-RAW (Figures S5A and S5C) and WS-EFF (Figures S6A and S6C) corresponded to locations previously characterized as humic- and fulvic-like fluorophores (Pifer and Fairey, 2014). Similarly, the maxima locations of Component 2 corresponded to protein-like fluorophores for BL-RAW (Figure S5B) and WS-EFF (Figure S6B) (Hudson et al., 2007). Component 4 in the BL-RAW model was considered negligible due to its location at maximum emission wavelengths and its low F_{MAX} values, which were insensitive to treatment. To gain further insight into the DBP precursors represented by each PARAFAC component and their removal by the nine types of CNTs, mean percent removals were calculated for each component (Table S6) based on F_{MAX} values for BL-RAW and WS-EFF (Table S5).

Using all nine possible combinations of triplicate samples for both raw and treated waters for a given CNT type, a conservatively large range of percent removal values were determined and used to calculate mean removals and 95% confidence intervals using the t-distribution (Table S5) due to small sample estimates of standard deviation. Removal of Components 1, 2

and 3 in WS-EFF by the CNTs all show similar trends in CNT performance to those observed for the removal of total THM formation potential (TTHMFP) and dihaloacetonitrile formation potential (DHANFP) (Figure S7A and S7B). Additionally, removal of Components 1 and 3 show strong correlations to DBPFP in BL-RAW (Figure S7D and S7E). Weak correlations were observed for total *N*-nitrosamine (TONO) formation potential removal (Figure S7C) and Components 2 and 4 in BL-RAW. For all nine CNT types in WS-EFF, Component 2 (protein-like fluorophores) had the highest mean percent removal (32-80%) of the three components. For six CNT types in BL-RAW, negative mean percent removals were calculated for Component 2, which was attibuted to a combination of low concentrations of protein-like compounds in BL-RAW source water and interferences of humic- and fulvic-like fluorophores skewing the magnitude of the fluorescent response, similar to the findings of others (Mayer et al., 1999). Additionally, the samples with negative mean percent removals also have relatively large 95% confidence intervals (12-339%). These observations illustrated the need for further investigation into the independence of individual PARAFAC components.

PARAFAC Component Correlations

Linear associations between PARAFAC components were tested for data sets incorporating samples treated with both low and high doses of CNTs. Correlations may be considered "weak" if $R < 0.5$, "strong" if $R > 0.8$, and "moderate" otherwise (Devore, 2004). As shown in Table S7 for the BL-RAW samples, the correlation is strong between Components 1 and 3 and moderate between Component 1 and Components 2 and 4. In constrast, correlations among Components 2, 3, and 4 are weak with R values between 0.43-0.49. For the WS-EFF samples, all correlations were strong between the three components, with R values of 0.85, 0.94, and 0.97. As such, even if protein-like fluorophore groups were the predominant precursors of

TONO, the influence of humic- and fulvic-like fluorophores would obscure this finding and produce poor correlations such as those observed in Figure S7C.

UV_{254} as a DBP Precursor Surrogate

Performing selected linear comparisons between single dependent variables and DBPFP revealed an interesting relationship between UV_{254} and TTHMFP (Figure S9A) and DHANFP (Figure S9B). While strong linear correlations existed between UV_{254} for the WS-EFF samples (TTHMFP, $R^2 = 0.74$ and DHANFP, $R^2 = 0.78$), those for BL-RAW samples had R^2 values less than 0.01, indicating the sensitivity of the absorbance scans were insufficient for characterization of TTHM and DHAN precursors. The sensitivity of UV_{254} measurements could possibly be improved by utilizing a 5 cm pathlength cuvette, instead of the 1-cm cuvette used in this study. However, fluorescence measurements utilize a much smaller pathlength of 0.5 mm while still maintaining a comparatively high sensitivity. This in addition to its usefulness across multiple water types (Figure S4) indicates fluorescence is a more robust DBP precursor surrogate than UV_{254}.

Table S1. Raw Water Characteristics

Water Type	**BL-RAW[1]**	**WS-EFF[2]**
pH	7.82	7.93
DOC[3] ($mg \cdot L^{-1}$)	2.33	5.98
UV_{254} (cm^{-1})	0.034	0.096
$I_{345/425}$ (QSE)[4]	5.16	14.25
Specific Conductivity ($\mu S \cdot cm^{-1}$)	155	535
Fluoride ($mg \cdot L^{-1}$)	0.11	0.47
Chloride ($mg \cdot L^{-1}$)	4.1	47.9
Bromide ($mg \cdot L^{-1}$)	0.11	0.16
Nitrate ($mg \cdot L^{-1}$)	1.3	23.9
Phosphate ($mg \cdot L^{-1}$)	ND[5]	0.29
Sulfate ($mg \cdot L^{-1}$)	8.0	47.2
Nitrite ($mg \cdot L^{-1}$)	ND	ND

[1]Raw intake water from Beaver Lake collected on July 7, 2014
[2]Effluent from the West Side Wastewater Treatment Plant collected on June 3, 2014
[3]Dissolved Organic Carbon
[4]Average fluorescence intensity at excitation and emission wavelengths of 325 nm and 425 nm respectively
[5]Not detected

Table S2. Manufacturer-specified properties of the selected carbon nanotubes.

CNT[1] Number	CNT Type	Supplier Description	Diameter (nm)	Length (□m)	S_{BET}[2] ($m^2 \cdot g^{-1}$)	Supplier
1	SW[3]	SWNTs (90%, regular length)	1-2	5-30	300-380	NAM, Inc. [4]
2		SW-DW CNTs 60	0.8-1.6	5-30	407	Cheap Tubes, Inc.
3	MW[5]	C-Grade MWNTs	1-3	80-150	NA[6]	NanoTechLabs, Inc.
4		MW CNTs 8 nm	2-5	10-30	500	Cheap Tubes, Inc.
5		MW CNTs 20-30 nm	5-10	10-30	110	Cheap Tubes, Inc.
6		95%, OD/ID: <10/2-7 nm	2-7	5-15	40-600	NAM, Inc.
7		95%, OD/ID: 30-50/5-15 nm	5-15	10-20	90-120	NAM, Inc.
8		PD30L5-20	15-45	5-20	200-400	NanoLab, Inc.
9		PD30L1-5	15-45	1-5	200-400	NanoLab, Inc.

[1]Carbon nanotube
[2]Supplier provided specific surface area from nitrogen adsorption isotherms using the Brunauer-Emmett-Teller (BET) model
[3]Single-walled
[4]Nanostructured & Amorphous Materials, Inc.
[5]Multi-walled
[6]Not Available

Table S3. Preliminary DBPFP Removal Testing

CNT Dose ($mg \cdot L^{-1}$)[1]	Water Type[2]	Average TTHMFP[3] Removal (%)	Average DHANFP[4] Removal (%)
0	BL-RAW	-	-
5	BL-RAW	14	-
50	BL-RAW	51	-
520	BL-RAW	98	-
0	BL-RAW	-	-
5	BL-RAW	26	37
50	BL-RAW	71	94
0	WS-EFF	-	-
5	WS-EFF	11	20
50	WS-EFF	67	96

[1]Single-walled CNTs were used in all dosed samples
[2]Beaver Lake raw water (BL-RAW) was collected on August 15, 2013 for first set of samples and April 5, 2014 for the second set. West Side WWTP effluent (WS-EFF) was collected on April 9, 2014.
[3]Average total trihalomethane formation potential based on duplicate samples
[4]Average dichloroacetonitrile formation potential based on duplicate samples

Table S4. Chlorine Residuals following filtration in batch studies

CNT Type	CNT Dose ($mg \cdot L^{-1}$)	Average Chlorine Residual ($mg \cdot L^{-1}$)	
		BL-RAW	**WS-EFF**
Blank	0	9.29	9.26
1	25	11.30	10.27
	50	11.47	10.18
2	25	13.83	11.32
	50	14.47	11.23
3	25	14.63	12.77
	50	14.90	12.31
4	25	14.09	12.03
	50	14.85	12.37
5	25	14.35	12.40
	50	14.22	10.72
6	25	15.30	12.65
	50	15.23	13.50
7	25	13.19	12.43
	50	14.00	13.18
8	25	14.76	11.20
	50	15.37	10.49
9	25	11.94	11.48
	50	13.80	10.80

Table S5. Fluorescence maximum (F_{MAX}) values

CNT Type	CNT Dose ($mg \cdot L^{-1}$)	Water Type						
		BL-RAW				WS-EFF		
		C1	C2	C3	C4	C1	C2	C3
Blank	0	9.7	5.1	3.0	1.8	17.1	10.1	9.5
		9.9	4.9	3.1	1.8	18.2	11.0	12.5
		9.9	4.3	3.0	1.8	18.0	10.9	12.1
1	25	4.2	1.9	1.1	1.5	8.1	3.5	4.8
		4.2	1.9	1.2	1.6	8.1	3.4	5.0
		4.3	2.0	1.2	1.4	8.4	3.6	5.8
	50	3.2	1.5	0.9	1.6	5.6	2.2	4.0
		3.2	1.5	0.9	1.3	5.6	2.2	4.4
		3.6	1.9	0.9	1.6	5.4	2.1	5.0
2	25	4.7	2.1	1.6	1.5	7.4	4.0	4.0
		4.9	2.1	1.6	1.5	7.5	4.1	4.2
		4.6	2.2	1.5	1.4	7.5	4.1	4.4
	50	3.2	1.6	1.0	1.3	4.4	2.3	2.6
		1.8	1.4	1.0	1.7	4.4	2.3	2.6
		4.0	3.2	1.6	1.7	4.5	2.4	2.9
3	25	8.0	6.5	2.3	2.4	13.1	6.4	9.4
		8.2	8.1	2.2	1.8	13.0	6.2	9.2
		7.8	4.5	2.2	1.8	13.6	6.5	10.1
	50	7.2	6.6	2.1	2.7	10.1	4.2	7.9
		5.2	2.0	1.6	1.6	9.9	4.0	6.8
		7.2	4.0	1.9	1.8	10.0	4.1	7.6
4	25	5.5	3.9	1.6	1.8	8.9	3.5	6.3
		5.6	6.0	1.6	2.0	7.8	3.1	4.7
		5.5	3.8	1.6	1.9	8.3	3.4	6.1
	50	4.2	3.2	1.2	1.6	5.5	2.1	3.9
		4.0	3.5	1.3	1.8	5.6	2.2	4.3
		4.1	3.3	1.2	1.7	5.7	2.2	4.4
5	25	6.1	6.9	1.9	1.8	10.9	4.8	8.2
		6.6	6.9	2.0	1.7	10.8	4.8	7.7
		6.7	9.9	2.0	1.8	11.1	5.0	9.1
	50	4.7	2.8	1.4	1.6	7.8	3.1	6.3
		5.5	4.9	1.7	1.8	7.9	3.2	6.2
		5.0	3.5	1.4	1.8	7.5	3.0	5.1
6	25	6.8	15.3	1.9	1.9	9.2	3.8	6.7
		6.7	13.3	1.9	1.9	9.2	3.9	6.4
		7.4	7.7	2.1	2.2	9.5	3.9	6.5

Table S5 Cont.

CNT Type	CNT Dose ($mg \cdot L^{-1}$)	Water Type						
		BL-RAW				WS-EFF		
		C1	C2	C3	C4	C1	C2	C3
6	50	4.9	3.0	1.3	1.8	6.7	2.5	5.3
		-	-	-	-	6.2	2.4	4.2
		5.6	14.3	1.5	1.8	6.6	2.5	5.3
7	25	9.5	10.5	2.7	2.0	14.2	7.1	10.7
		10.2	11.1	2.9	2.0	14.1	7.2	10.7
		7.9	5.2	2.3	1.9	14.1	7.3	10.9
	50	7.8	17.6	2.1	2.0	11.6	5.1	10.5
		6.7	9.8	2.0	1.9	11.6	5.2	9.0
		8.9	10.8	2.2	2.3	11.7	5.3	9.2
8	25	-	-	-	-	8.9	3.4	7.1
		6.5	7.3	1.7	2.1	9.2	3.6	7.5
		6.1	10.7	1.7	1.7	10.1	3.9	8.4
	50	4.7	8.0	1.5	1.7	6.7	2.5	5.8
		3.7	3.4	1.2	1.4	6.6	2.3	7.4
		4.5	10.0	1.3	1.6	6.5	2.4	5.3
9	25	5.7	8.6	1.5	1.7	9.7	4.0	7.4
		5.5	6.2	1.6	1.7	9.4	3.9	7.1
		5.6	6.8	1.8	2.3	9.5	3.8	7.8
	50	4.7	8.5	1.4	1.7	6.5	2.4	4.8
		4.1	7.5	1.3	2.1	6.6	2.4	5.0
		4.5	4.1	1.4	1.6	6.6	2.5	5.2

Table S6. Mean percent removal of each PARAFAC component

Water Type	CNT Type	Dose = 25 mg·L^{-1} CNTs			
		C1[1]	C2	C3	C4
BL-RAW	1	57 ± 2.5[2]	59 ± 11	62 ± 2.3	16 ± 16
	2	52 ± 5.0	55 ± 14	48 ± 6.3	19 ± 7.8
	3	19 ± 8.4	-37 ± 123	27 ± 6.1	-11 ± 48
	4	44 ± 2.3	2 ± 89	47 ± 2.6	-7 ± 12
	5	34 ± 10	-70 ± 129	36 ± 7.2	2 ± 5.6
	6	29 ± 12	-160 ± 252	35 ± 13	-11 ± 30
	7	6 ± 33	-92 ± 200	12 ± 27	-9 ± 14
	8	36 ± 7.1	-93 ± 129	44 ± 2.6	-5 ± 28
	9	43 ± 4.0	-53 ± 102	46 ± 10	-5 ± 55
WS-EFF	1	54 ± 6.2	67 ± 5.4	53 ± 30	-[3]
	2	58 ± 4.1	62 ± 5.5	62 ± 18	-
	3	25 ± 10.9	40 ± 11	14 ± 43	-
	4	53 ± 11.3	69 ± 7.5	49 ± 35	-
	5	38 ± 7.6	54 ± 8.1	25 ± 43	-
	6	47 ± 6.6	64 ± 5.5	42 ± 25	-
	7	20 ± 7.5	32 ± 10	4 ± 40	-
	8	47 ± 13	66 ± 10	31 ± 42	-
	9	46 ± 6.5	63 ± 6.1	33 ± 33	-

[1]Components 1-4 represented as C1-C4
[2]95% confidence intervals calculated from maximum range of possible removal values
[3]Model for WS-EFF were only validated with a maximum of three components

Table S6 Cont.

Water Type	CNT Type	Dose = 50 mg·L^{-1} CNTs			
		C1	C2	C3	C4
BL-RAW	1	66 ± 7.5	65 ± 18	70 ± 1.2	15 ± 25
	2	69 ± 30	55 ± 62	60 ± 27	10 ± 32
	3	34 ± 31	8 ± 145	39 ± 21	-12 ± 86
	4	58 ± 3.5	29 ± 21	59 ± 4.9	4 ± 21
	5	49 ± 12	20 ± 76	51 ± 12	2 ± 18
	6	47 ± 11	-89 ± 339	54 ± 9.6	1 ± 3.6
	7	21 ± 31	-175 ± 292	31 ± 14	-16 ± 32
	8	56 ± 15	-54 ± 206	56 ± 14	13 ± 23
	9	55 ± 9.0	-44 ± 145	54 ± 8.0	1 ± 38
WS-EFF	1	69 ± 4.1	80 ± 3.5	60 ± 27	-
	2	75 ± 3.0	78 ± 3.4	75 ± 14	-
	3	44 ± 6.4	61 ± 5.9	33 ± 37	-
	4	68 ± 4.3	80 ± 3.6	62 ± 20	-
	5	56 ± 5.7	71 ± 4.9	47 ± 32	-
	6	63 ± 6.5	77 ± 4.6	56 ± 27	-
	7	34 ± 6.2	51 ± 8.2	14 ± 52	-
	8	63 ± 5.0	77 ± 4.7	44 ± 47	-
	9	63 ± 3.9	77 ± 3.4	55 ± 21	-

Table S7. Linear correlations (R) between components of BL-RAW and WS-EFF PARAFAC Models

Water Type		Components		
		C1	**C2**	**C3**
BL-RAW	**C2**	0.51	-	-
	C3	0.97	0.43	-
	C4	0.54	0.47	0.49
WS-EFF	**C2**	0.97	-	-
	C3	0.94	0.85	-

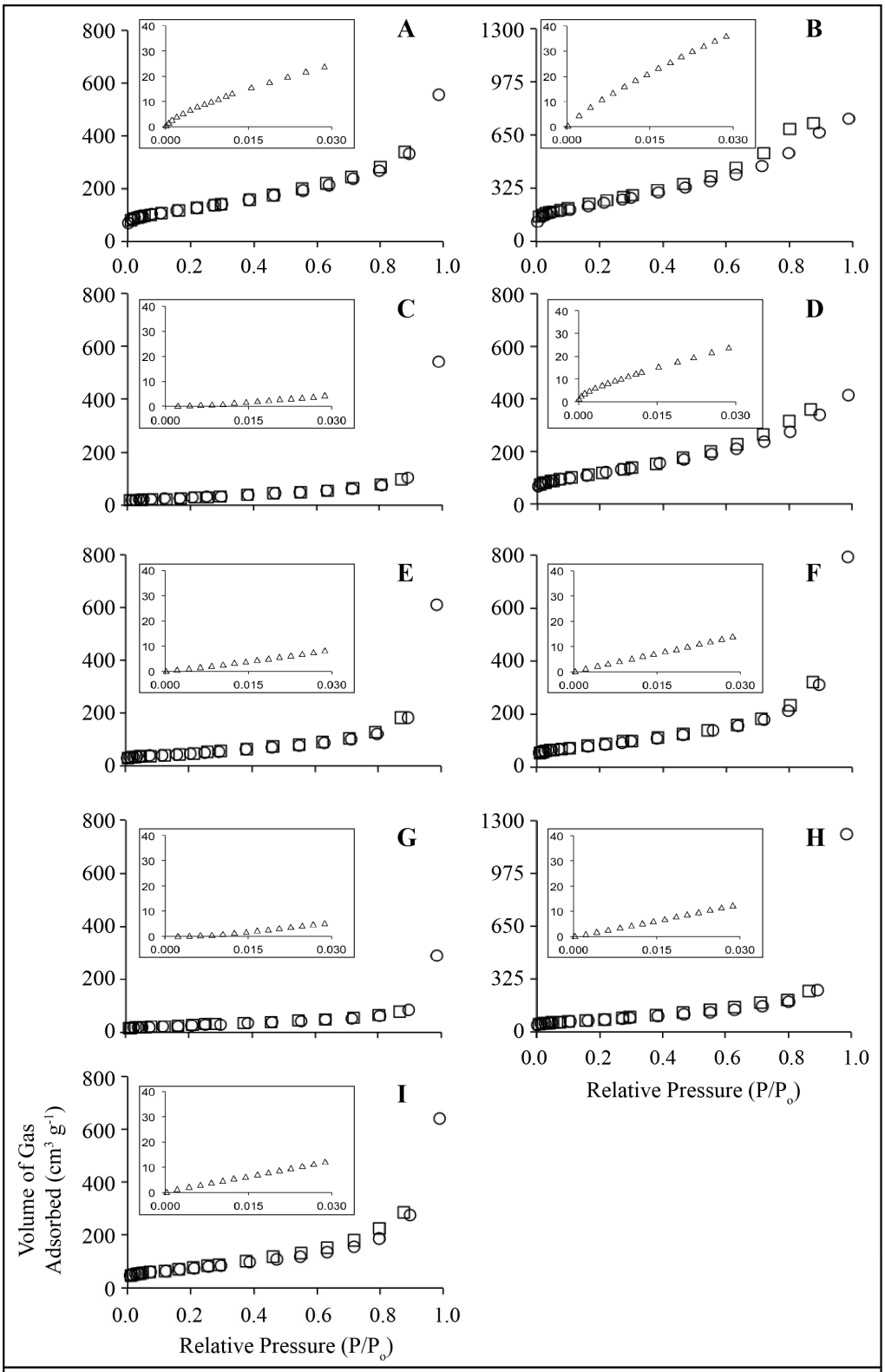

Figure S1. Gas Adsorption Isotherms for CNT Types 1-9 (Figures S1A-S1I). Nitrogen gas adsorption (○) and desorption (□) loops are accompanied by inset carbon dioxide gas adsorption (△) loops. Units are constant for all isotherms.

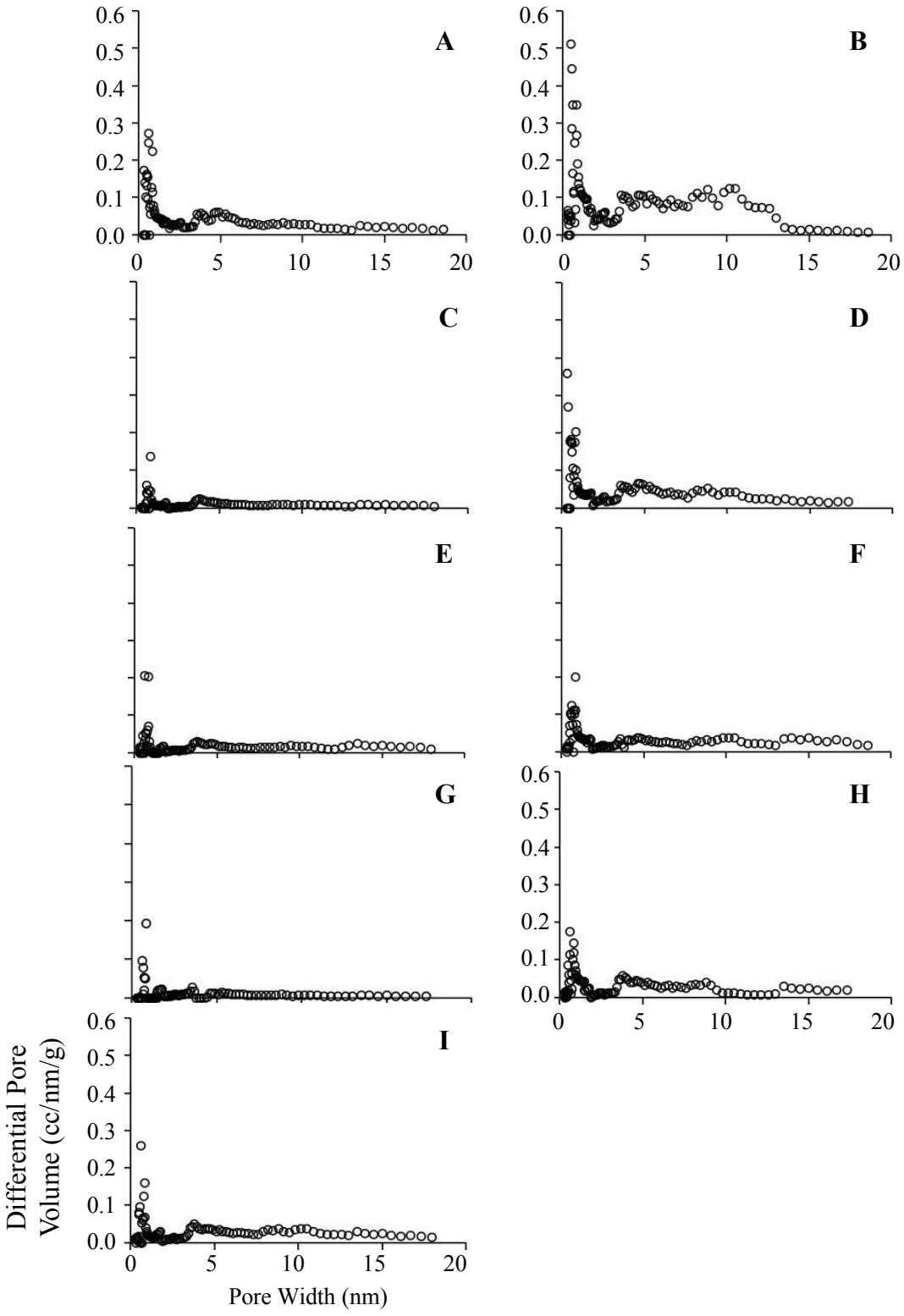

Figure S2. Pore volume distributions for CNT Types 1-9 (Figures S2A-S2I), all with identical scales

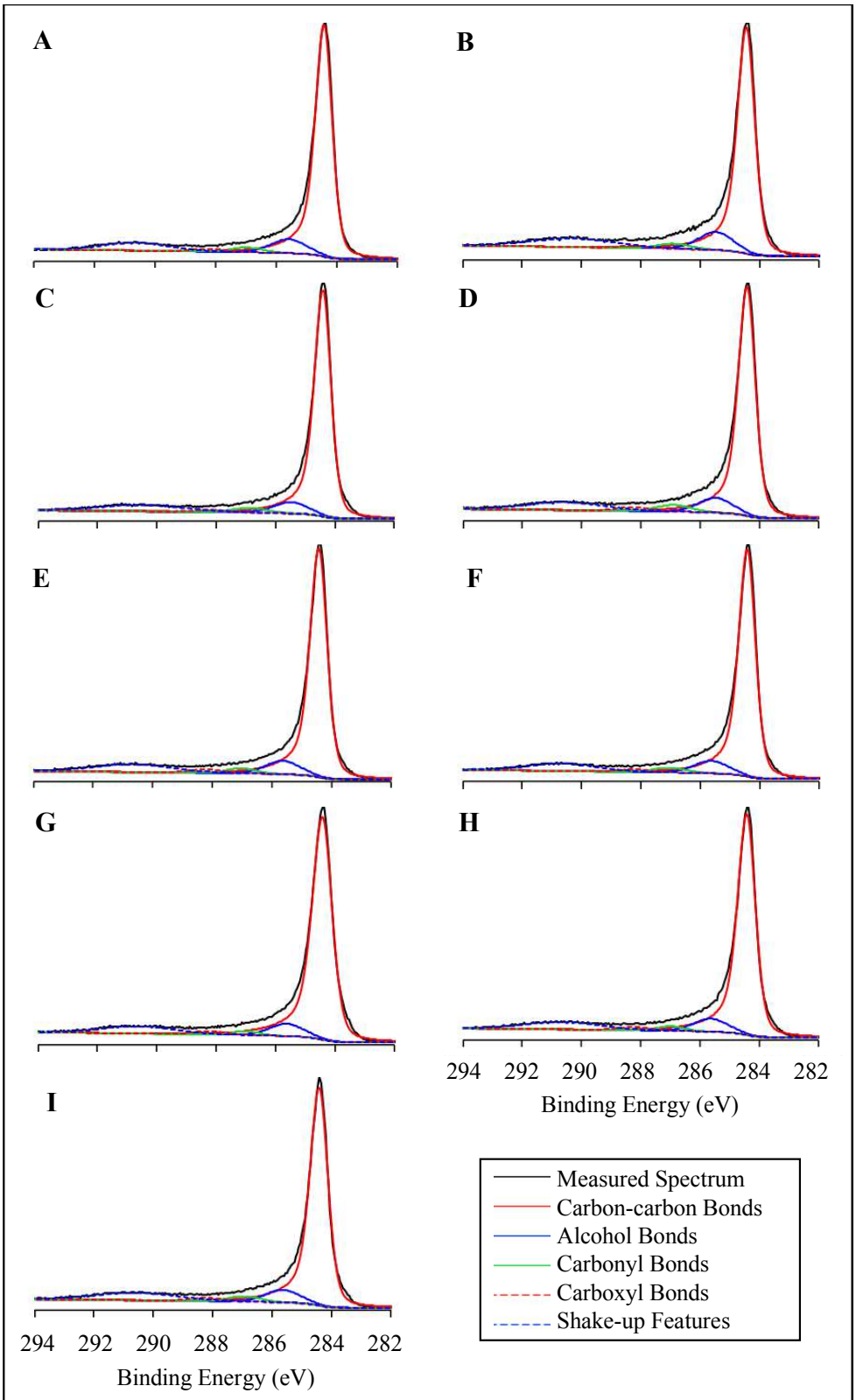

Figure S3. Deconvolutions of Carbon Spectra from XPS Measurements for CNT Types 1-9 (Figures S3A-S3I)

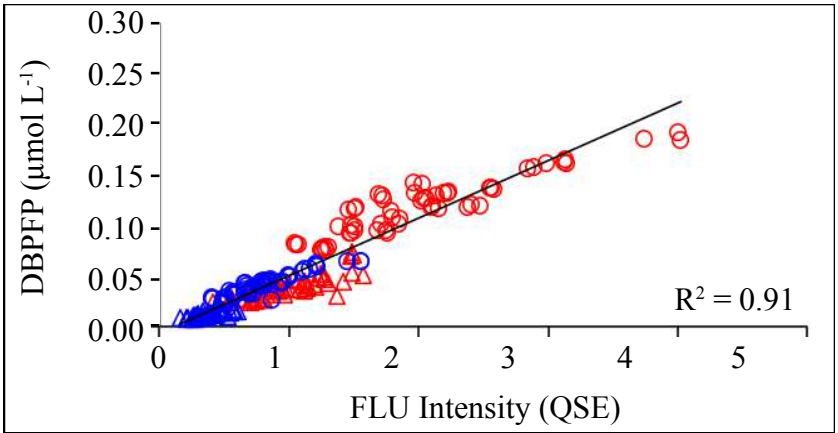

Figure S4. Linear regression of fluorescence at $R_{MAX}{}^{2}$ excitation-emission wavelength pairs against TTHMFP in BL-RAW (△) and WS-EFF (○) and DHANFP in BL-RAW (△) and WS-EFF (○).

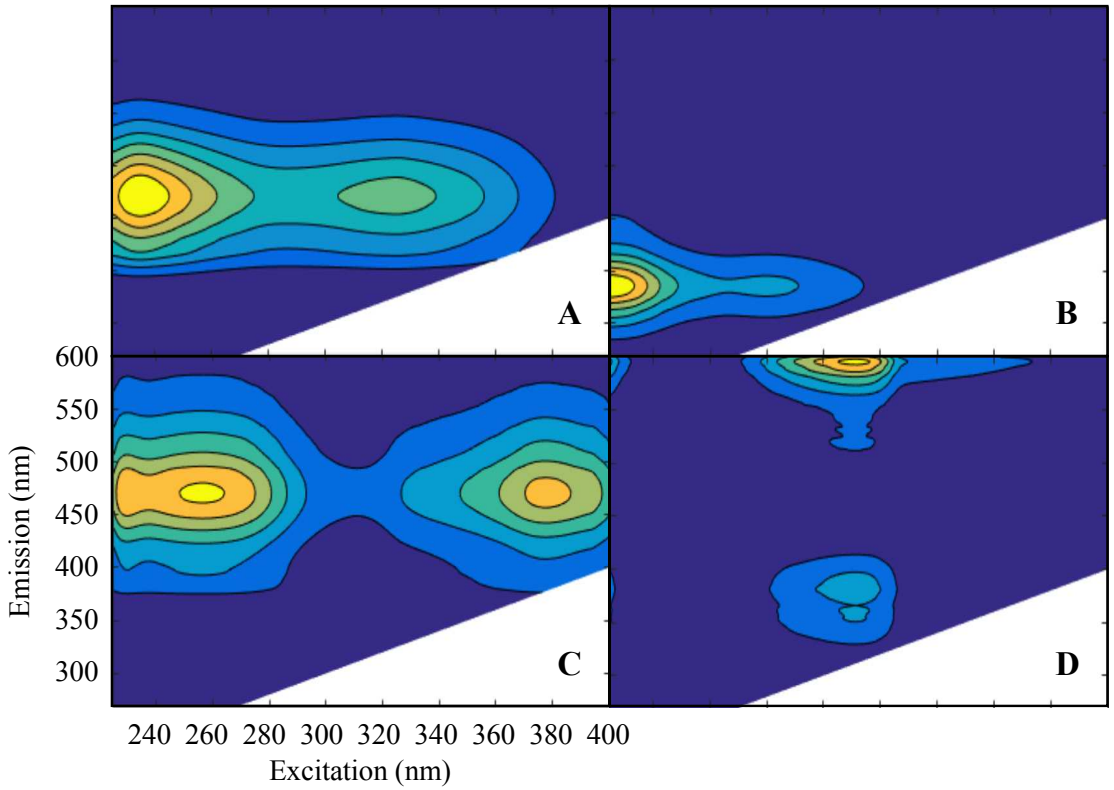

Figure S5. PARAFAC Component EEMs for Beaver Lake Raw Water. A) Component 1, B) Component 2 and D) Component 4 utilize the axes specified in C) Component 3.

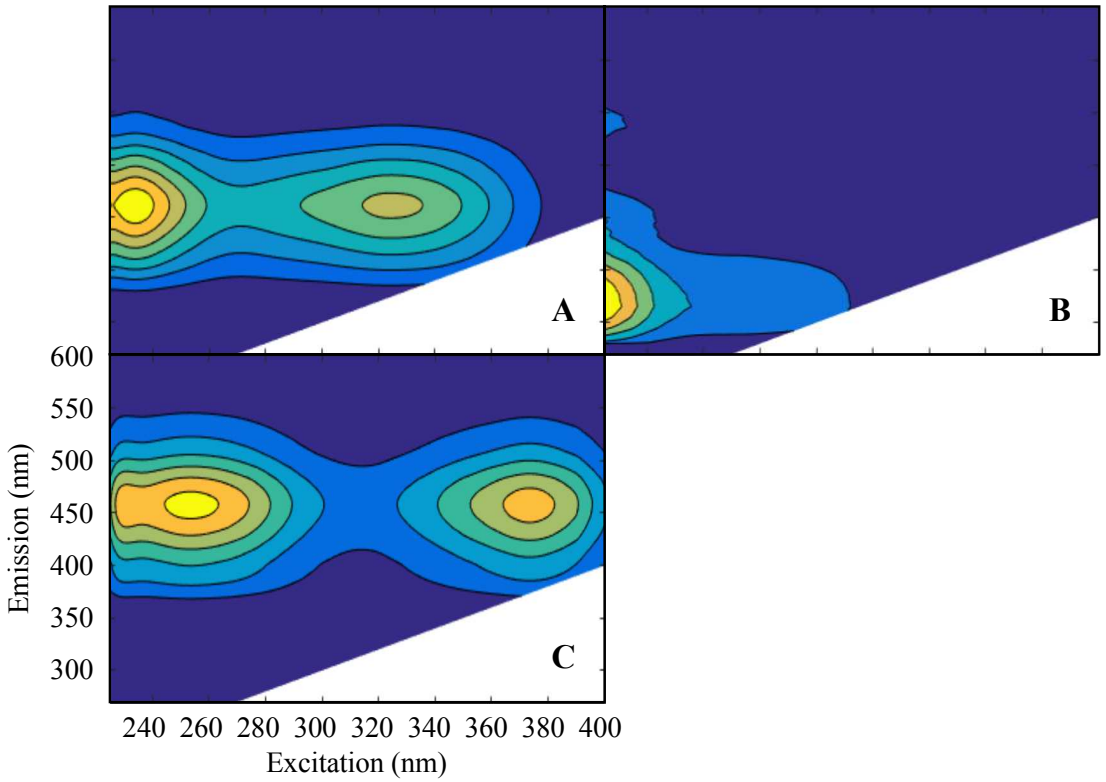

Figure S6. PARAFAC Component EEMs for West Side WWTP Effluent. A) Component 1 and B) Component 2 utilize the axes specified in C) Component 3.

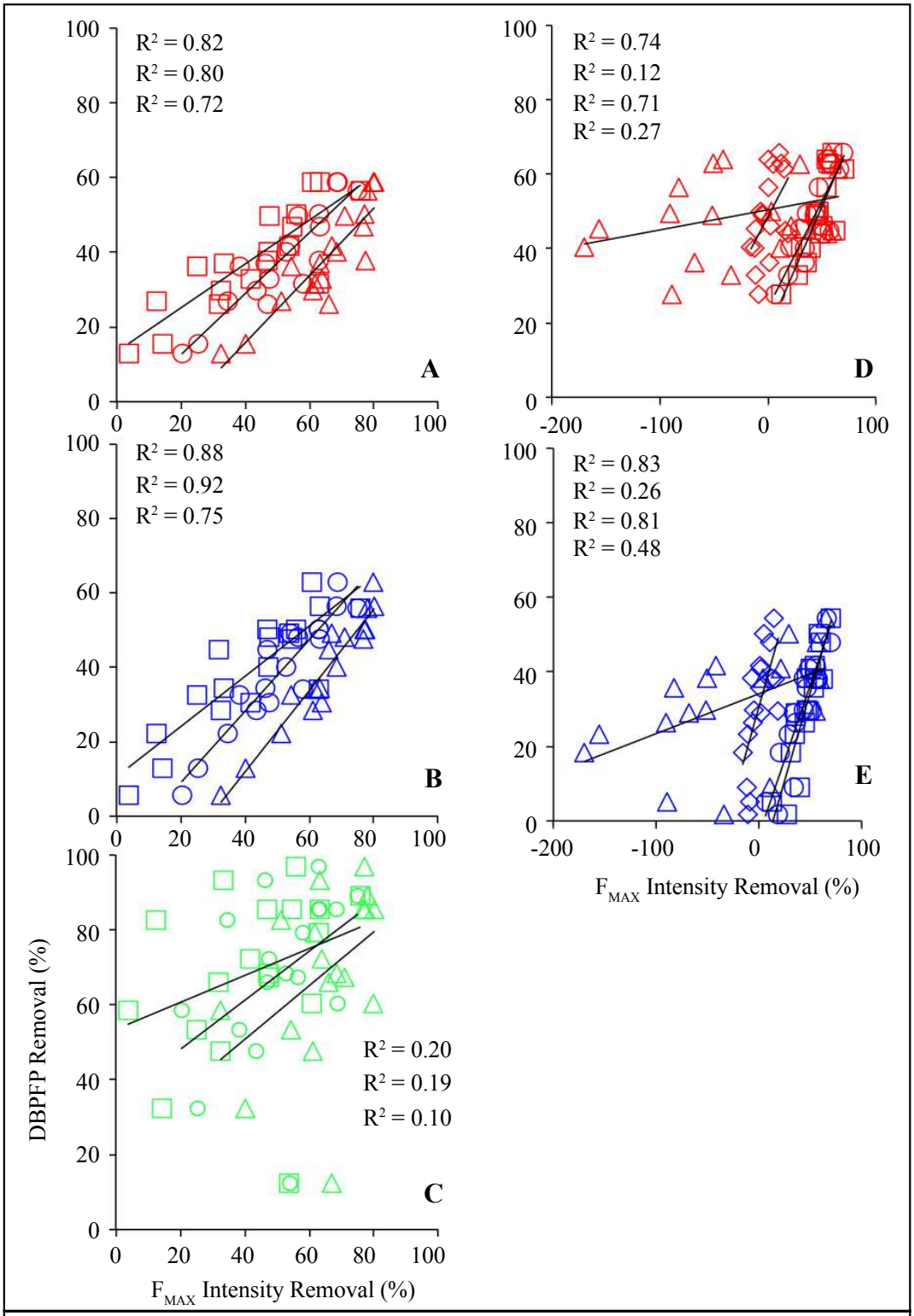

Figure S7. Linear regressions of DBPFP percent removal against percent removal of F_{MAX} of PARAFAC Components 1 (○), 2 (△), 3 (□), and 4 (◇) for TTHMFP, DHANFP, and TONOFP (Figures S8A-S8C) in WS-EFF and TTHMFP and DHANFP (Figures S8D and S8E) in BL-RAW. R^2 values appear according to numerical Component order.

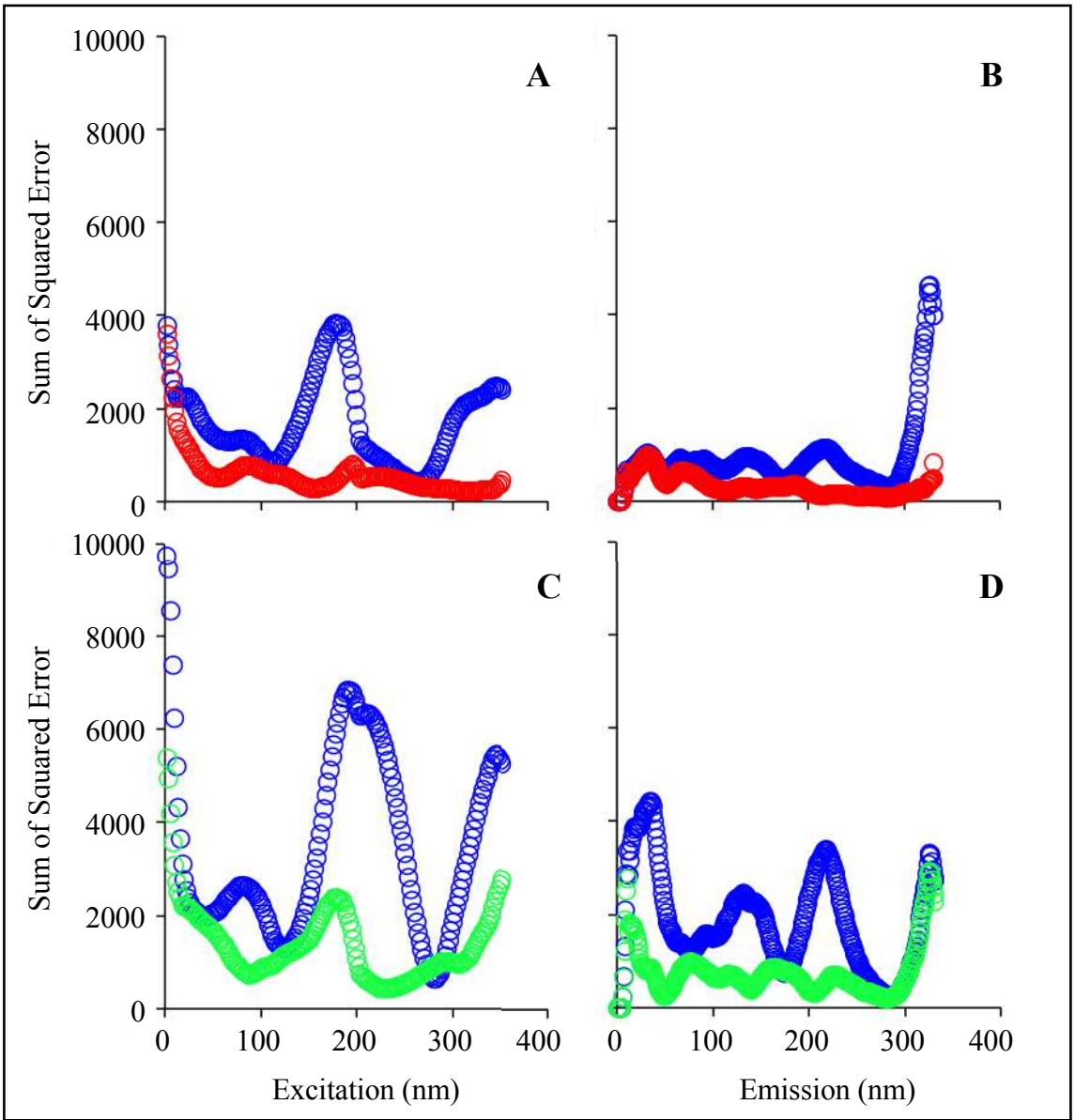

Figure S8. Sum of squared errors for excitation and emission wavelengths based on PARAFAC models with varying quantities of components. Two component (○) and 4 component (○) models were validated for BL-RAW (Figure S9A and S9B). Two component and three component (○) models were validated for WS-EFF (Figure S9C and S9D).

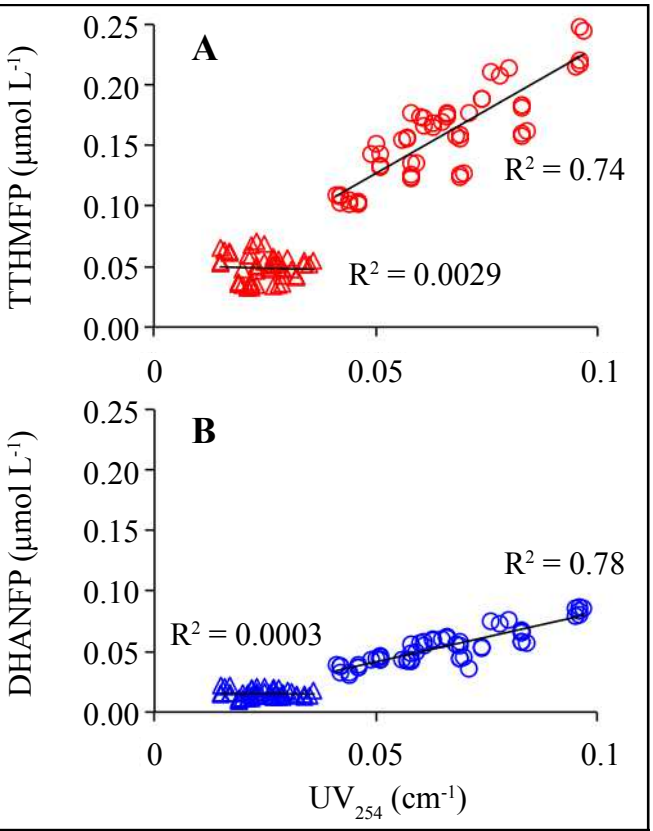

Figure S9. Linear regression of TTHMFP in BL-RAW (○) and WS-EFF (△) (Figure S10A) and DHANFP in BL-RAW (○) and WS-EFF (△) (Figure S10B).

References

Ago, H., Kugler, T., Cacialli, F., Salaneck, W. R., Shaffer, M. S. P., Windle, A. H. and Friend, R. H., 1999. Work functions and surface functional groups of multiwall carbon nanotubes. Journal of Physical Chemistry B 103 (38), 8116-8121.

Andersen, C. M. and Bro, R., 2003. Practical aspects of PARAFAC modeling of fluorescence excitation-emission data. Journal of Chemometrics 17 (4), 200-215.

Cory, R. M., Miller, M. P., McKnight, D. M., Guerard, J. J. and Miller, P. L., 2010. Effect of instrument-specific response on the analysis of fulvic acid fluorescence spectra. Limnology and Oceanography-Methods 8, 67-78.

Devore, J. L., 2004. Probability and statistics for engineering and the sciences, 6, Brooks/Cole, Thomson Learning, Belmont, CA.

Do, T. D., Chimka, J. R. and Fairey, J. L., 2015. Improved (and singular) disinfectant protocol for indirectly assessing organic precursor concentrations of trihalomethanes and dihaloacetonitriles. Environmental Science & Technology 49 (16), 9858-9865.

Hudson, N., Baker, A. and Reynolds, D., 2007. Fluorescence analysis of dissolved organic matter in natural, waste and polluted waters - A review. River Research and Applications 23 (6), 631-649.

Kovtyukhova, N. I., Mallouk, T. E., Pan, L. and Dickey, E. C., 2003. Individual single-walled nanotubes and hydrogels made by oxidative exfoliation of carbon nanotube ropes. Journal of the American Chemical Society 125 (32), 9761-9769.

Kristiana, I., Lethorn, A., Joll, C. and Heitz, A., 2014. To add or not to add: The use of quenching agents for the analysis of disinfection by-products in water samples. Water Research 59, 90-98.

Kundu, S., Xia, W., Busser, W., Becker, M., Schmidt, D. A., Havenith, M. and Muhler, M., 2010. The formation of nitrogen-containing functional groups on carbon nanotube surfaces: a quantitative XPS and TPD study. Physical Chemistry Chemical Physics 12 (17), 4351-4359.

Mayer, L. M., Schick, L. L. and Loder, T. C., 1999. Dissolved protein fluorescence in two Maine estuaries. Marine Chemistry 64 (3), 171-179.

McKnight, D. M., Boyer, E. W., Westerhoff, P. K., Doran, P. T., Kulbe, T. and Andersen, D. T., 2001. Spectrofluorometric characterization of dissolved organic matter for indication of precursor organic material and aromaticity. Limnology and Oceanography 46 (1), 38-48.

McPhail, M. R., Sells, J. A., He, Z. and Chusuei, C. C., 2009. Charging nanowalls: adjusting the carbon nanotube isoelectric point via surface functionalization. Journal of Physical Chemistry C 113 (32), 14102-14109.

Okpalugo, T. I. T., Papakonstantinou, P., Murphy, H., McLaughlin, J. and Brown, N. M. D., 2005. High resolution XPS characterization of chemical functionalised MWCNTs and SWCNTs. Carbon 43 (1), 153-161.

Pifer, A. D. and Fairey, J. L., 2014. Suitability of organic matter surrogates to predict trihalomethane formation in drinking water sources. Environmental Engineering Science 31 (3), 117-126.

Ramanathan, T., Fisher, F. T., Ruoff, R. S. and Brinson, L. C., 2005. Amino-functionalized carbon nanotubes for binding to polymers and biological systems. Chemistry of Materials 17 (6), 1290-1295.

Shapiro, S. S. and Wilk, M. B., 1965. An analysis of variance test for normality (complete samples). Biometrika 52, 591-611.

Singh, B., Fang, Y., Cowie, B. C. C. and Thomsen, L., 2014. NEXAFS and XPS characterisation of carbon functional groups of fresh and aged biochars. Organic Geochemistry 77, 1-10.

Wang, H., Zhou, A., Peng, F., Yu, H. and Yang, J., 2007. Mechanism study on adsorption of acidified multiwalled carbon nanotubes to Pb(II). Journal of Colloid and Interface Science 316 (2), 277-283.

Yan Yan, H. and Terentjev, E. M., 2012. Dispersion of carbon nanotubes: mixing, sonication, stabilization, and composite properties. Polymers 4 (1), 275-95.

Zepp, R. G., Sheldon, W. M. and Moran, M. A., 2004. Dissolved organic fluorophores in southeastern US coastal waters: correction method for eliminating Rayleigh and Raman scattering peaks in excitation-emission matrices. Marine Chemistry 89 (1-4), 15-36.

Zhang, Z., Pfefferle, L. and Haller, G. L., 2014. Comparing characterization of functionalized multi-walled carbon nanotubes by potentiometric proton titration, NEXAFS, and XPS. Chinese Journal of Catalysis 35 (6), 856-863.